Bearings-Only Tracking Automation for a Single Unmanned Underwater Vehicle

by

Danica Lee Middlebrook

B.S. Systems Engineering
United States Naval Academy, 2005

Submitted to the Department of Mechanical Engineering
in partial fulfillment of the requirements for the degree of

Master of Science in Mechanical Engineering

at the

MASSACHUSETTS INSTITUTE OF TECHNOLOGY

June 2007

Author .....
Department of Mechanical Engineering
May 18, 2007

Certified by .....
Christopher Dever
Senior Member, Technical Staff, C.S. Draper Laboratory
Thesis Supervisor

Certified by .....
Michael Triantafyllou
Professor of Mechanical and Ocean Engineering
Thesis Supervisor

Accepted by .....
Lallit Anand
Professor of Mechanical Engineering
Chair, Committee on Graduate Students

Bearings-Only Tracking Automation for a Single Unmanned Underwater Vehicle

by

Danica Lee Middlebrook

Submitted to the Department of Mechanical Engineering
on May 18, 2007, in partial fulfillment of the
requirements for the degree of
Master of Science in Mechanical Engineering

Abstract

Unmanned underwater vehicles have various missions within civilian, military and academic sectors. They have the ability to explore areas unavailable to manned assets and to perform duties that are risky to humans. In particular, UUVs have the ability to perform bearings-only tracking in shallow areas near shorelines. This thesis presents a guidance algorithm for this particular mission. This thesis first presents a Modified Polar Extended Kalman Filter for the estimation problem. Bearings-only tracking is a nonlinear problem that requires some sort of estimator to determine the target state. The guidance algorithm is developed based on the relative positions of the observer and the target. In order to develop the guidance algorithm, the effectiveness of a variety of course maneuvers are presented. The effectiveness of these maneuvers are analyzed both quantitatively and qualitatively. The results from this analysis is incorporated into the final guidance algorithm. This thesis also evaluates the developed guidance algorithm through a series of simulation experiments. The experiments explore a variety of scenarios by varying speed, geometry and acoustic environment. The results of the experiments are analyzed based on estimation errors and detection time. The final conclusions indicate that some of the geometries are more favorable than others. In addition, the degree of noise in the acoustic environment affects the range of the UUV's sensors and the UUV's ability to perform bearings-only tracking for an extended period of time. In addition, the desired speed ratio is one in which the observer is either the same speed as or slower than the target.

Thesis Supervisor: Christopher Dever
Title: Senior Member, Technical Staff, C.S. Draper Laboratory

Thesis Supervisor: Michael Triantafyllou
Title: Professor of Mechanical and Ocean Engineering

Acknowledgments

This thesis would not have been completed with out the help and support of a diverse group of people.

I first want to thank Chris Dever, my supervisor at Draper, for his hard work in providing guidance in both my research and my writing. Thanks also goes to Michael Triantafyllou, my advisor at MIT for keeping me on the right track.

I want to thank the Draper fellows that my time here as overlapped with, for provided some much needed breaks and laughter.

For support while I have been here in Boston, I would like to thank the girls from my small groups at Park Street Church. Thank you for your prayers and friendship. I would especially like to thank Katie Jenks for her friendship and for all of the dinners that we have shared together.

Thanks also goes out to Livia King and Karen Zee, my two swimming buddies for getting me out of the office on a mostly weekly basis. Thank you for your time and understanding and good luck as you continue your research.

Of course I want to thank my parents, Rod and Jan Adams and my sister, Brianne Adams, for their love and support and the rest of my extended family. Thank you for being there for me, and understanding when I didn't want to talk about my work.

Let me not forget to thank my husband, Justin Middlebrook. Thank you for your love, support and faith in me. It's been a tough two years, mostly apart and I look forward to growing in our life together.

And finally: *And whatever you do, whether in word or deed, do it all in the name of the Lord Jesus, giving thanks to God the Father through him.* - **Colossians 3:17**

This thesis was prepared at The Charles Stark Draper Laboratory, Inc., under Independent Research and Development Project Number 21181-001.

Contents

List of Figures

List of Tables

Chapter 1

Unmanned Underwater Vehicles

Autonomous vehicles allow humans to explore places that were previously unreachable to them. They also provide access into areas that are too dangerous or too risky for humans to enter. This is constant through all environments but especially underwater. The realm under the oceans is mostly a mystery to humans. However, unmanned underwater vehicles (UUVs) provide new and insightful information about this underwater world.

1.1 Missions for UUVs

The missions for UUVs are vast and diverse. They have topographical, archeological, oceanagraphic, reconnaissance and other types of operations. UUVs have been used to photograph the Titanic, examine steam vents, map the ocean floor and detect mines, to name a few specific missions. They provide access to the depths of the ocean as well as the shallows.

UUVs can withstand pressures that manned vehicles can not. They can also operate in littoral areas without risking human lives. Littoral areas are the ocean areas near the shore. The smaller size of the UUVs allows them to operate in areas too shallow for larger vessels.

These differences allow UUVs to perform missions that are either impossible for a larger platform to accomplish or that are too dangerous for a human to perform. UUVs have missions in both civilian and military arenas. In 2004, the US Navy released an update to its UUV Master Plan in which the main missions for UUVs included maritime reconnaissance, undersea search and survey (both for oceanographic and mine countermeasures), communication/navigation network nodes and anti-submarine warfare [29]. Current missions for UUVs include inspection and identification as well as the mine countermeasures. Many of the recent developments have been in these two areas. The UUVs are intended to be modular and able to perform multiple missions depending on the circuitry installed.

The UUVs also vary in size depending on the mission. They range from man portable size (diameter of 3-9 inches) to a large class UUV (diameter $\geq$ 36 inches). The two intermediate classes are the light weight vehicle (LWV) and the heavy weight

vehicle (HWV). The different classes have different endurance times and are used for various missions. For example, mine countermeasures could be performed by either the LWV (operation area clearance) or the HWV (clandestine reconnaissance). Large class, LWVs and HWVs can perform oceanographic surveys. The choice of class depends on the specific area and endurance required for the survey. The large UUVs are the primary class for anti-submarine warfare (ASW) and payload delivery [29].

1.2 Choke Point Monitoring

Unmanned underwater vehicles have a potential to be a force multiplier for various platforms. As a force multiplier, the UUVs would allow for more missions with the same number of manned platforms. Within the mission of anti-submarine warfare, the UUVs could monitor choke points and harbors to track and trail the enemy. This usage would allow other assets to be otherwised engaged until the UUV handed off its subject. When the UUV hands off its contact, it transfers the information it has collected to another platform, which will then continue the tracking and make the decision whether or not to engage the contact.

Choke points are areas in which there are few possible courses through which a vehicle can travel. Some examples include the Strait of Gibralter or the Suez Canal. Due to the depth of these channels, any vehicle exiting them would have few course options until it gets out into deeper water. In order to monitor these areas, possible platforms include UUVs. Due to the reduced nature of choke points and harbors, they are easier to monitor than the wide open ocean. A sensor network would allow for potential interesting targets and contacts to be monitored and tracked as soon as they are leaving port or a choke point.

1.2.1 Bearings-Only Tracking

In order to be able to track an enemy submarine or ship, the UUV must be able to perform target motion analysis (TMA). This is the ability to determine the range, course and speed of a target. In order to maintain secrecy, the only information used would be the bearings between the observer and the target, resulting in bearings-only target motion analysis (BO-TMA). The bearing between the observer and the target is the angle at which the observer detects the target (see Figure 1.1). Bearings-only TMA uses passive sensors, which allows the UUV (or any other vessel) to observe without being detected itself [30]. This type of underwater TMA has typically been performed by submarines or surface ships performing anti-submarine tactics. The ability to perform TMA with UUVs would allow the UUVs to aquire and track the target sooner than conventional means.

The UUVs could be part of a sensing network that monitors choke points and delivers information to another vessel that is waiting further out from the choke point. Figure 1.2 demonstrates the UUV laying out the sensor field as well as tracking a target. The UUV could be cued either by a sensor field or a third party source such as another UUV or a manned vessel. The sensor field might be laid out in advance

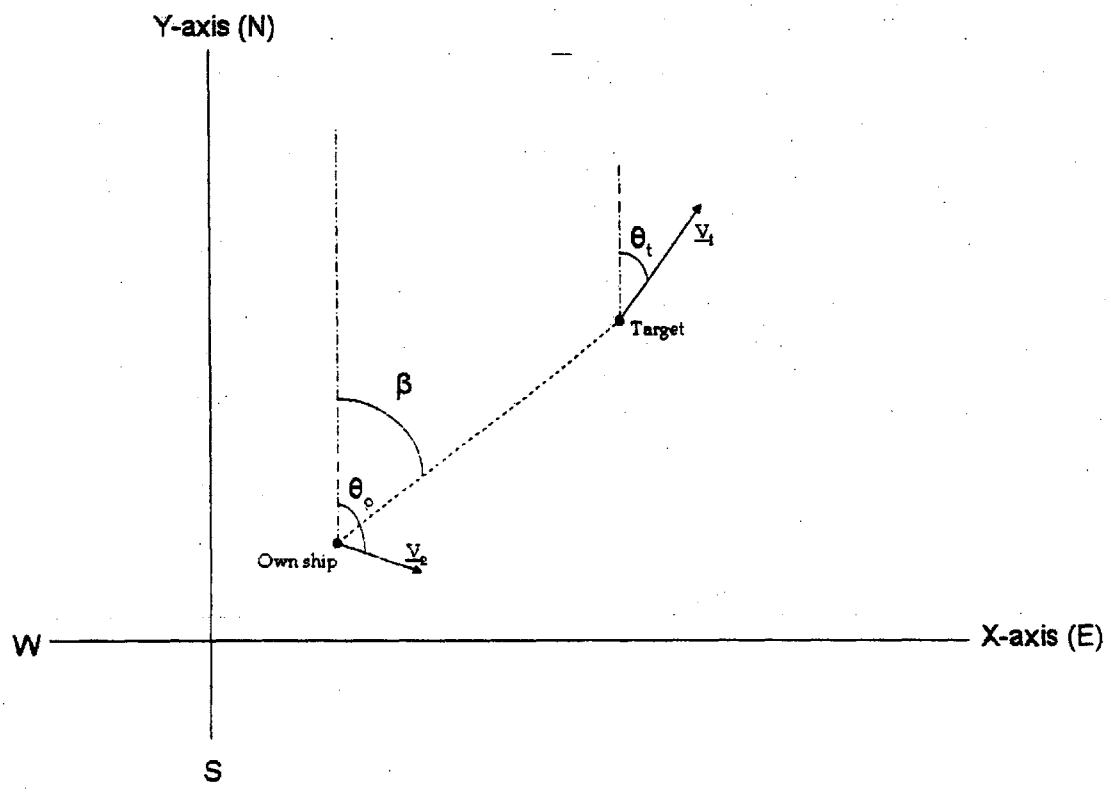

Figure 1.1: Basic geometry definition of bearing between the observer (own ship) and the target. All angles are measured from with respect to 000 as north. β is the bearing or line of sight angle between the observer and the target from the point of view of the observer. v_t is the velocity of the target (speed and course) while v_o is the velocity of the observer. θ_t is the target's course and θ_o is the observer's course.

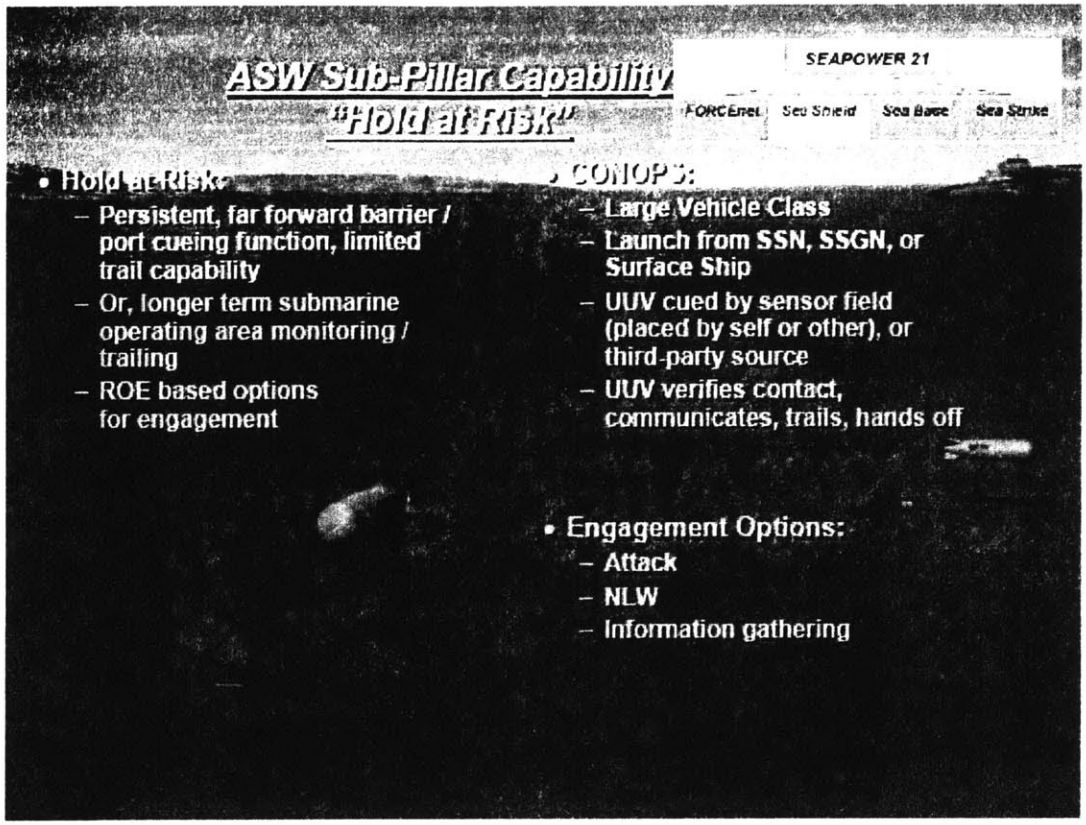

Figure 1.2: Anti-Submarine Warefare Sub-Pillar Concept of Operation "Hold at Risk" from the Navy Unmanned Undersea Vehicle Master Plan [29]

by the same UUV, another UUV, a diver or some other method.

This thesis looks at creating a framework in which to perform bearings-only tracking with UUVs. In order to do so, some sort of processing must be done with the noisy bearings only data. The different types of maneuvers that are performed to accomplish bearings-only tracking are analyzed and used as a starting point to codify BO-TMA for UUVs.

1.3 Problem Statement

The fundamental question that this thesis looks at is whether or not UUVs have the capability to perform BO-TMA without human interaction. Some of the main challenges within this thesis is to develop a proper estimation algorithm as well as develop a guidance system for the UUV to perform the required maneuvers to track the target. The estimation algorithm is inherently linked to the guidance system in this application because the guidance system uses the output of the estimation algorithm in making its decisions. This capability is useful because it allows the UUVs to be utilized in tracking targets sooner than a manned asset might be able to.

In order to determine whether or not BO-TMA is feasible using UUVs, an es-

timation algorithm was chosen. For the purpose of this research, a modified polar extended Kalman filter was chosen. The reasons for this choice will be further explored in a later chapter. Figure 1.3 presents the proposed flow chart for the control of the vehicle. The chart includes the various aspects of the required mission. In addition to tracking another vessel, the UUV must be aware of its surroundings (avoiding obstacles and avoiding counter-detection) as well as able to complete its mission and report the information that it has gathered to the rest of the area.

The main contributions of this thesis are a working Modified Polar Extended Kalman Filter and a guidance system which allows the UUV to track another vehicle based on sensor information and the surrounding environment.

1.4 Literature Review

The problem of performing and optimizing bearings-only target motion analysis has been extensively studied. There has not been much work with performing BO-TMA with UUVs specifically, but with submarines in general. Much of the work done in target motion analysis was done prior to the major push in work in UUVs in the past ten years. The previous work focused more on the problems of estimation, observability and processing rather than on the actual platform performing the BO-TMA. The work done in bearings-only target motion analysis fall into a few different categories. Typical work has focused on the observability of the problem, what type of estimation to use in processing the data and the optimal observer maneuvers.

The first area in which much work has been done in the bearings-only target motion analysis problem is that of observability. Observability for this problem is defined as the existence of a unique tracking solution [3]. Becker presents both a derivation for a linear approach to the Nth-order dynamics target case [2] and further simplification and application of the observability conditions to more general cases [3]. Fogel and Gavish also obtained the observability conditions, in which the observer must have an order of trajectory dynamic greater than that of the target [10]. For example, to observe the trajectory of a constant velocity target, the observer must have some sort of acceleration (either change in course or change in speed). Jauffret and Pillon build on both of these works, examining the nature of observability in passive target motion analysis [15]. For angles-only TMA, a maneuver is required by the observer to obtain observability. The observability problem influences both the choice of estimator as well as the optimal maneuver problem.

A natural extension of the observability problem is to use some form of estimation algorithm. There are various approaches to this problem: the maximum likelihood estimator (MLE), the pseudo-linear estimator (PLE) and Kalman filters. A fourth approach to the problem is the graphical method, which was commonly used prior to computers and is still taught to submarine officers. Two examples of the graphical method are the Ekelund range and the Spiess range [30]. These were devised by two naval officers in the 1950s and were the first two complete bearings-only TMA solutions.

The other three types of solutions are numerical estimators. The pseudo-linear

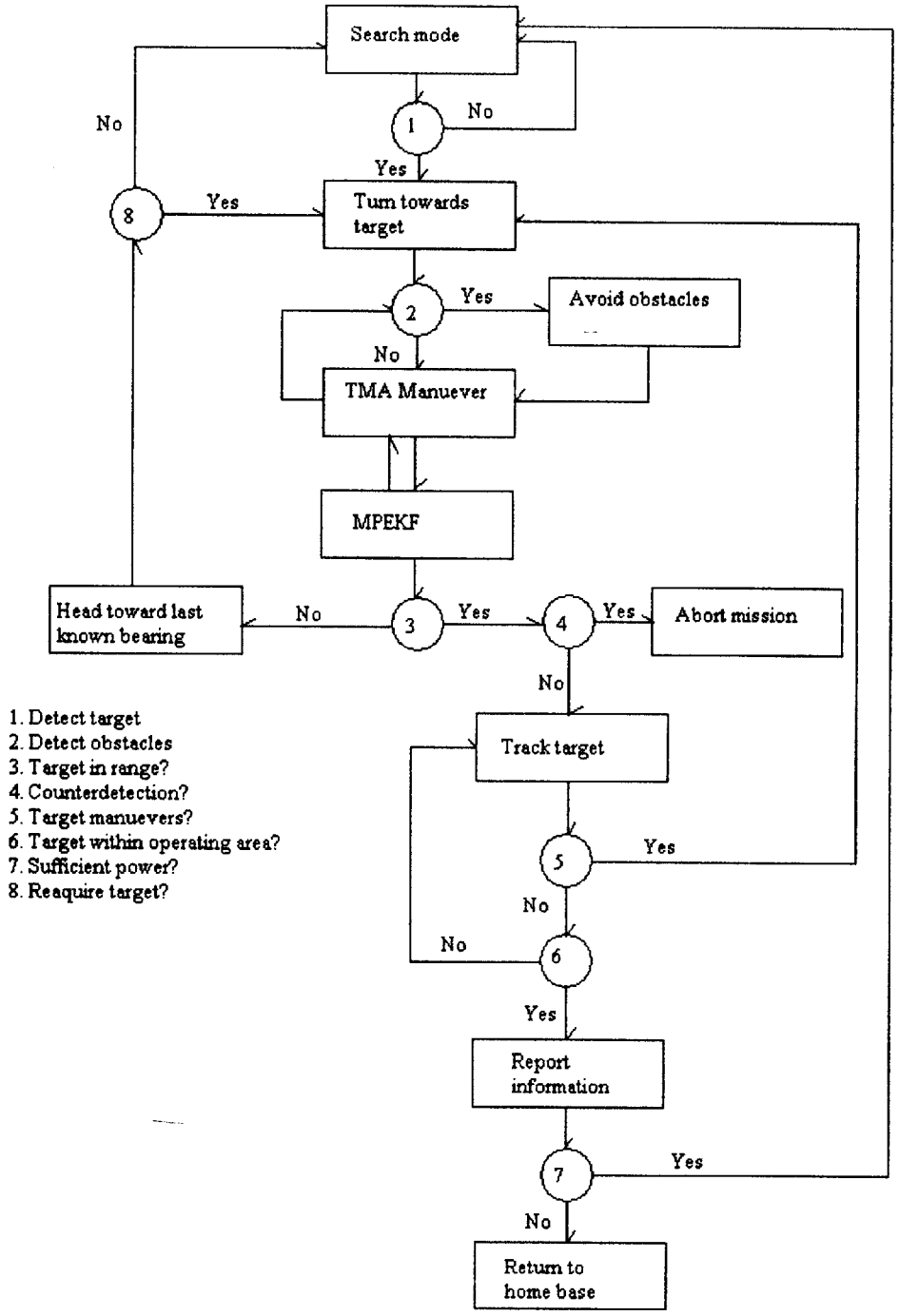

Figure 1.3: Proposed Problem Flowchart

estimator is an explicit method which provides solutions as a funtion of the measurements [4, 25]. However, the PLE has known bias and is not very efficient. Pham presents a quadratic estimator that is similar to the PLE but lacks the bias of the PLE [25]. The PLE is also used in a comparison study of performance against the MLE [22]. Within this study, it is determined that the PLE has increased bias as the effective noise increases, making it an unsuitable estimator for this project.

Nardone, et. al. further explore a closed form solution that is applied in a similar method to the MLE [21]. In Berman's work, a reliable MLE is found that is a hybrid of sorts that works at high ranges [5]. Both the maximum likelihood estimator and the pseudo-linear estimator are nonrecursive batch methods.

These batch methods are compared to recursive methods (which are based in Kalman filtering) [14, 8]. The main difference between the two methods is the method of linearization. The batch processing was determined to be more accurate at extremely long ranges than the recursive processing [14].

The recursive methods consist of the use of Kalman filters. The earliest work in this area developed a Modified Polar Extended Kalman filter (MPEKF) to use in lieu of a regular cartesian Kalman Filter [1]. This modification allows for the state equations to be decoupled and for the measurement to be linear. The modified polar coordinates better reflect the coordinates in which the problem was set. Moorman and Bullock made modifications to the extended Kalman filter to remove most of the bias that was present [20]. All three estimators have been the basis of much of the work done in bearings-only TMA. The MPEKF has advantages in that it uses less processing power. The batch processing of the MLE improves the long range estimation. For the purpose of this thesis, the MPEKF was chosen.

In addition to the work done in observability and estimation, there has also been a focus on optimizing the maneuvers performed by the observer (or own ship). Fawcett used the Cramer-Rao lower bound to predict the behavior of an MLE in response to various maneuvers in order to chose the course that would optimize the performance of the estimator [9]. Passerieux and Van Cappel used optimal control theory to determine the maneuver that minimizes a criterion based on the Fisher information matrix. They determined that [24]

> the obtained optimal (or very close to optimal) observer trajectories are as follows: 1) with the range accuracy criterion, a > trajectory with two legs of equal lengths, target near the broadside direction on both legs and direction of the second leg such that bearing rate is maximized, 2) with the global accuracy criterion, a smooth Z trajectory composed of three legs of approximately equal lengths, and 3) in both cases the averaged observer motion is oriented towards the target.

Kronhamn used an adaptive ownship motion control based on the multihypothesis cartesian Kalman filter to determine optimal maneuvers [17]. S.E. Hammel has done much of her work in the area of BO-TMA. Her doctoral thesis focuses specifically on optimal observer motion for the nonlinear tracking problem [13]. Like much of the other work done in this area, it shows that there is a trade-off between increasing bearing rate and decreasing range in the observer maneuvers. LeCadre and Trémois

took a different approach in determining optimal observer motion within bearings-only tracking. They used dynamic programming within a hidden Markov model of the problem [6, 7, 26].

In 2004, the US Navy released its Unmanned Underwea Vehicle Master Plan which was the culmination of many hours of work done by various committees and workshops. It presents an overall view of the current uses of UUVs and a plan for future development [29]. This document presents an overview of the research timelines and areas of necessary development and research. In his master's thesis, Mierisch examined and developed a situational awareness algorithm for UUVs [19]. His basic premise was for the UUV to use its measurements of the contact's motion to determine whether or not it had been detected. Mierisch used probability and known observations of passive and hostile behavior to make this determination.

Another area of work that is vital to bearings-only tracking is that of underwater acoustics. Underwater acoustics provides of the basis of the bearing measurements. Both Lurton and Urick present a comprehensive introdution to underwater acoustics and sound [18, 28]. Building on Lurton and Urick's work as well as their own practical experience, the professors of *Underwater Acoustics and Sonar* at the United States Naval Academy have created their own set of course notes based on this information [27]. This work provides the basis for the environmental simulation within this thesis.

1.5 Thesis Organization

This thesis will further delve into the choice and the development of the Modified Polar Extended Kalman Filter in Chapter 2. The guidance algorithm will be presented in Chapter 3, along with its development. Chapter 4 examines the simulation environment and experimental setup. Also, this chapter will further explain the models chosen to represent the underwater environment. Chapter 5 will look at the performance of the algorithm and present the results of the simulations. The final chapter, Chapter 6, will draw conclusions from these results and present further areas of research.

Chapter 2

Modified Polar Extended Kalman Filter

There are various approaches to the bearings-only estimation problem. The Modified Polar Extended Kalman Filter (MPEKF) was chosen for this thesis in part due to the commonality of the Kalman filter. The lower processing power and recursive structure required by the MPEKF also makes it a more appropriate candidate for UUVs with limited power. In addition, the proposed situation does not require extreme long range estimation (the area in which the maximum likelihood estimator outperforms the MPEKF). Therefore, this thesis focuses on the use of the MPEKF for its estimation algorithm.

2.1 State Space and Measurement Models

Bearings-only tracking is inherently a nonlinear problem. The nonlinearity can either be in the state equations or in the measurement equations. If a traditional cartesian Kalman filter is used, the state dynamics are linear while the measurement relationships are nonlinear. The traditional cartesian state vector consists of the relative position and relative velocity of the target in both the x and y direction.

Transforming the problem into modified polar coordinates, on the other hand, causes the state equations to be nonlinear but the measurement matrix to be linear. The state vector then contains the bearing, the bearing rate, the range rate divided by range and the reciprocal of range of the target from the observer's perspective. The measurement vector has been simplified since it is solely concerned with the bearing.

Another benefit of using modified polar coordinates is that the state vector is partially decoupled. The only component that is not observable prior to an observer maneuver is the reciprocal of range. This allows the state estimates to behave as one would theoretically expect, even in the face of errors, unlike the Cartesian coordinates [1].

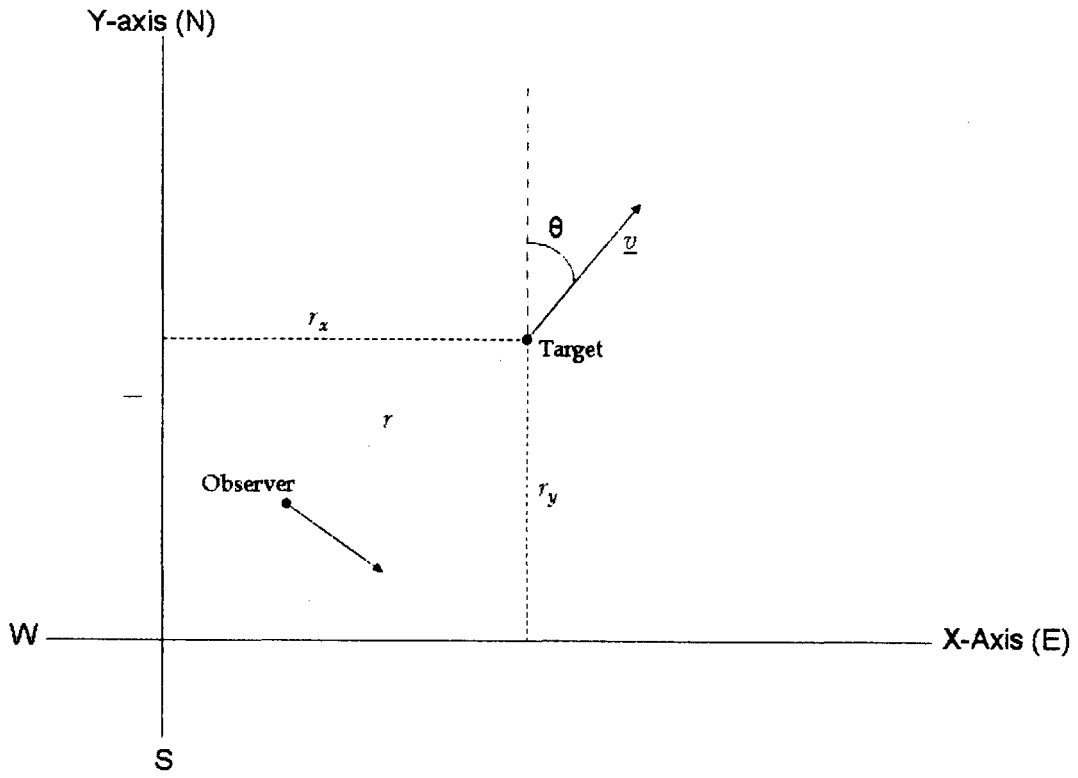

Figure 2.1: Visual representation of the target state vector where r_x is the target's x-position, r_y is the target's y-position, θ is the target's course, v is the target's speed and r is the range between the observer and the target.

2.1.1 State space coordinate transformation

Since the algorithm uses the modified polar coordinate system, the transformation from the target and observer state vectors is presented. The initial absolute state space vector for the target is given by

$$x_t = \begin{bmatrix} r_{xt} \\ r_{yt} \\ v_t \\ \theta_t \end{bmatrix} \tag{2.1}$$

where r_{xt} and r_{yt} are the target position, v_t is the target speed and θ_t is the target course in cartesian coordinates (Figure 2.1). The state vector for the observer is similar. The modified polar state vector, on the other hand is defined by

$$y = \begin{bmatrix} y_1 \\ y_2 \\ y_3 \\ y_4 \end{bmatrix} = \begin{bmatrix} \dot{\beta} \\ \dot{r}/r \\ \beta \\ 1/r \end{bmatrix} \tag{2.2}$$

where r is the range between the observer and the target and β is the bearing angle from the observer to the target. The modified polar extended Kalman filter uses the modified polar (MP) state vector for its estimation. However, the information that is of interest to the observer is the course and speed of the target, as well as its position. Therefore, transformations between the two coordinate systems are included within the MPEKF. The cartesian state vector used in Aidala and Hammel's work consists of the relative position and velocity of the target with respect to the observer [1]. The formation of this vector from the aforementioned target state vector is given as follows:

$$x = \begin{bmatrix} x_1 \\ x_2 \\ x_3 \\ x_4 \end{bmatrix} = \begin{bmatrix} v_t \sin(\theta_t) - v_o \sin(\theta_o) \\ v_t \cos(\theta_t) - v_o \cos(\theta_o) \\ r_{xt} - r_{xo} \\ r_{yt} - r_{yo} \end{bmatrix} \tag{2.3}$$

where v_t is the target's speed, v_o is the observer's speed, θ_t is the target's course, θ_o is the observer's course, r_{xt} and r_{yt} are the target's position and r_{xo} and r_{yo} are the observer's position.

Once this state vector is obtained, it can easily be transformed into the y-coordinate system and vice versa. Since the observer state is assumed known with reasonable accuracy, the target information can be pulled from the transformed x state vector. The transformations between the coordinate systems are as follows:

$$x = f_x[y] = \frac{1}{y_4} \begin{bmatrix} y_2 \sin(y_3) + y_1 \cos(y_3) \\ y_2 \cos(y_3) - y_1 \sin(y_3) \\ \sin(y_3) \\ \cos(y_3) \end{bmatrix} \tag{2.4}$$

$$y = f_y[x] = \begin{bmatrix} [x_1 x_4 - x_2 x_3] / [x_3^2 + x_4^2] \\ [x_1 x_3 + x_2 x_4] / [x_3^2 + x_4^2] \\ \tan^{-1}[x_3/x_4] \\ 1/\sqrt{x_3^2 + x_4^2} \end{bmatrix}. \tag{2.5}$$

2.2 Filter Equations

The filter equations are based on the general discrete time Kalman filter relations from Gelb's *Applied Optimal Estimation* [12] and the derivation of the MPEKF found in Aidala and Hammel's *Utilization of Modified Polar Coordinates for Bearings-Only*

Tracking [1]. The filter is initialized using

$$\hat{y}_0 = \text{initial estimate of the MP state vector} \tag{2.6}$$
$$P_0 = \text{initial estimate of the MP state vector error covariance matrix.} \tag{2.7}$$

Once the filter is initialized, the propagation phase commences. This filter does not include any process noise [1]. In the propagation phase between measurements,

$$\hat{y}^- = f[y] \tag{2.8}$$
$$A_y = \frac{\partial f[y]}{\partial y} \tag{2.9}$$
$$P^- = A_y * P * A_y^T. \tag{2.10}$$

where the function f is defined as

$$f[y] = \begin{bmatrix} [S_1 S_4 - S_2 S_3] / [S_3^2 + S_4^2] \\ [S_1 S_3 + S_2 S_4] / [S_3^2 + S_4^2] \\ y_3 + \tan^{-1}[S_3/S_4] \\ y_4/\sqrt{S_3^2 + S_4^2} \end{bmatrix} \tag{2.11}$$

where

$$S_1 = y_1 + y_4[w_1 \cos(y_3) - w_2 \sin(y_3)] \tag{2.12}$$
$$S_2 = y_2 + y_4[w_1 \sin(y_3) + w_2 \cos(y_3)] \tag{2.13}$$
$$S_3 = (\Delta t) y_1 + y_4[w_3 \cos(y_3) - w_4 \sin(y_3)] \tag{2.14}$$
$$S_4 = 1 + (\Delta t) y_2 + y_4[w_3 \sin(y_3) + w_4 \cos(y_3)] \tag{2.15}$$

in which w_i is relative acceleration term that is dependent on the characteristics of the motion of both the target and observer and Δt is the time between measurement steps (assumed to be 1 for this thesis). The measurement matrix for this particular EKF is

$$H = [0, 0, 1, 0] \tag{2.16}$$

because β is measured directly.

Using the measurements, the filter estimate is updated using the following equations:

$$K = P^- H^T [H P^- H^T + R] \tag{2.17}$$
$$P = [I - KH] P^- \tag{2.18}$$
$$\hat{y} = \hat{y}^- + K[z - H\hat{y}^-] \tag{2.19}$$

where R is the measurement noise covariance and z is the actual sensor measurement of bearing β.

2.3 Observability

Due to the fact that the bearing is the only measurement that the filter is receiving, neither the range nor its reciprical is observable without some sort of maneuver. A passive sensor gives bearing information and possibly frequency information but is unable to obtain range information. An active sensor on the other hand, provides range information since it is known how long it takes the energy to travel to the target and back to the sensor. A passive sensor is just receiving energy. The other parts of the state vector are observable because they can be derived from the bearing measurements. In order for the state vector to be fully observerable, the observer needs to perform some type of maneuver. In this case, the observability of the range is intuitive.

The necessity of an observer maneuver can also been seen by looking at the system dynamics [12]. The A matrix is a partial differentiation of Equation (2.11). This is made up of the S functions given in Equations (2.13) through (2.15). When both the target velocity and the observer velocity are constant, the w terms are equal to zero because the target's and observer's accelerations are zero. If the w terms are equal to zero, the y_4 term falls out of the S functions, thereby having no effect on the other states. State $y_4 = \frac{1}{r}$, so the reciprical of range is not observerable when neither the target nor the observer have any acceleration. However, when the observer performs a known maneuver, the w terms are now nonzero and y_4 will drive β (the direct measurement), causing $\frac{1}{r}$ to be observable through β.

The final method of looking at the observability is to look at it from a linear algebra point of view. In this method, the rank of the observability matrix determines how many states in the state vector are observable [16]. The observability matrix is shown as

$$O = \begin{bmatrix} H \\ H \cdot A \\ H \cdot A^2 \\ H \cdot A^3 \end{bmatrix} \tag{2.20}$$

where H is the measurement array given in Equation (2.16) and A is the matrix given in Equation (2.10). During a straight segment of the observer's motion

$$O = \begin{bmatrix} 0 & 0 & 1 & 0 \\ x & x & 1 & 0 \\ x & x & 1 & 0 \\ x & x & 1 & 0 \end{bmatrix} \tag{2.21}$$

where x represents any non-zero value. This matrix has $rank(O) = 3$ and therefore is not fully observable. As can be seen by the observability matrix itself, the final column is always zero, indicating that y_4 is unobservable. When the observer is in

the middle of a maneuver, the observability matrix is

$$O = \begin{bmatrix} 0 & 0 & 1 & 0 \\ x & x & 1 & x \\ x & x & 1 & x \\ x & x & 1 & x \end{bmatrix} \tag{2.22}$$

again where x represents any non-zero value. In this case $rank(O) = 4$, indicating a fully observable state vector.

All three of the methods demonstrate that a maneuver is required in order to have a fully observable state vector of the target.

The next chapter will focus on the development of the guidance algorithm and logic through the used of the modified polar extended Kalman filter.

Chapter 3

Guidance algorithm

This chapter looks at the process of developing the guidance algorithm. The various steps building towards the final guidance system include a conceptual flow chart, an examination of the effect of a wide range of maneuvers and the incorporation of the general rule of balancing increasing the bearing rate and decreasing the range, verified by a detailed maneuver examination, into the final algorithm. Each of these steps will be further explored in the different sections of this chapter. The guidance algorithm is one of the main contributions of this thesis.

3.1 Guidance concept

Figure 3.1 is a presentation of the conceptual high-level guidance flow chart. This section further examines the guidance components that the flow chart contains.

The initial concept for the guidance begins with the UUV in a search mode, waiting to detect a target or to be cued. This mode allows the UUV to either be in a sweeping mode or a loitering mode. There are two options for the search mode: the UUV looks for contacts or waits to be cued. When the UUV is looking for contacts, it will most likely make continuous sweeps of a specified area. An example of this would be to "mow the law" in long paths. On the other hand, a sensor network could have been previously laid. In this scenario, the UUV will loiter until the sensor network alerts it to a coming contact. The sensor network then passes on the target's course, speed and position information to the UUV.

Once the UUV either detects a target or is cued by the sensor network, it turns towards an intercept course with the target. The UUV will either use the information from its own sensors or the information passed from the sensor network to determine the intercept course. Once the UUV has turned towards the target, the bearings-only TMA goes into effect.

Running concurrently with the bearings-only target motion analysis (BO-TMA) is an obstacles avoidance regime. The BO-TMA maneuvers are intertwined with the updates to the Kalman filter, in which both affect the other. Once the maneuvers are complete and the UUV has a good tracking estimate, it falls in behind the target and continues to track it until it either goes out of range, maneuvers, goes out of

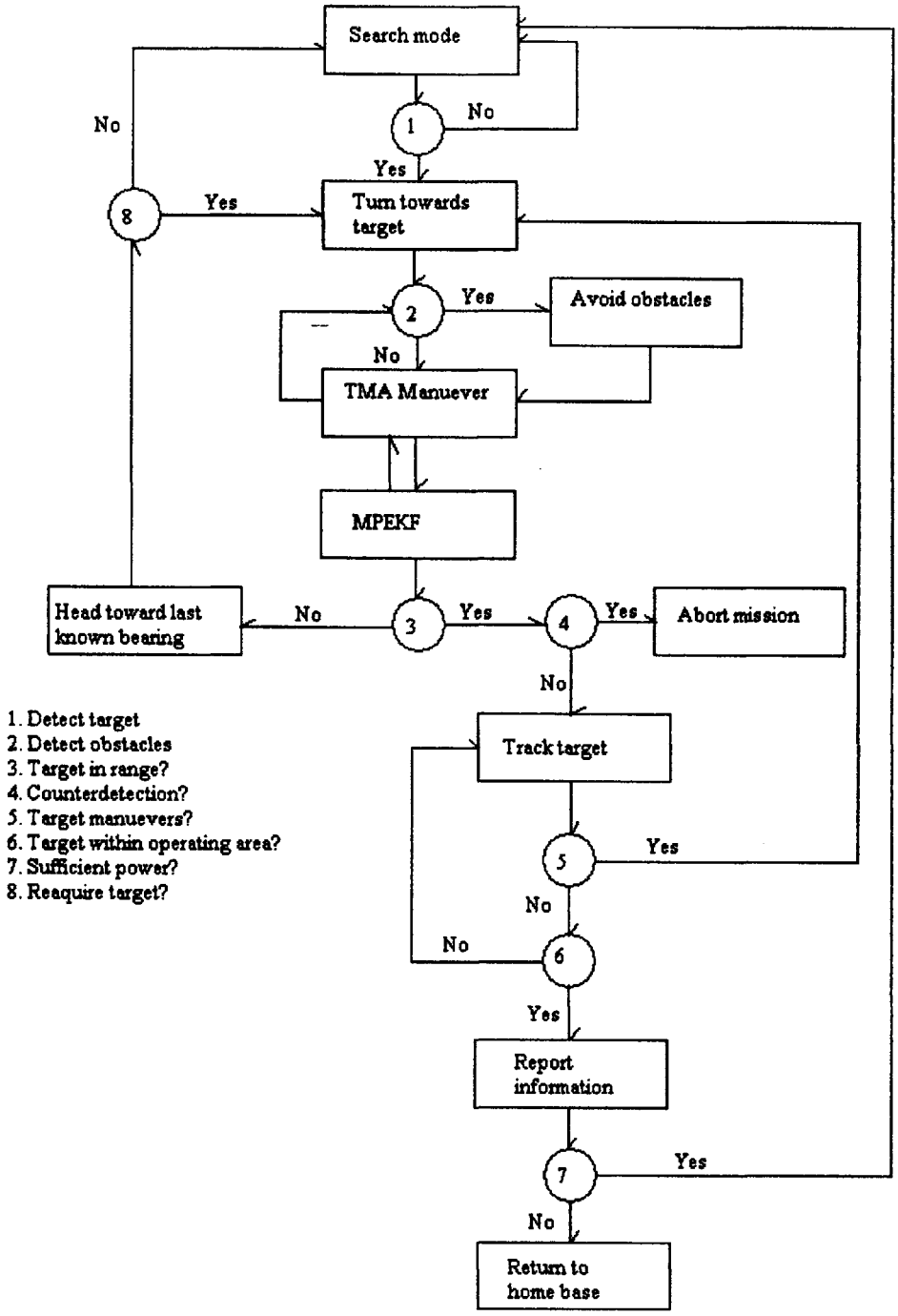

Figure 3.1: Conceptual Guidance Pseudo-Code

the UUV's operating area or counterdetects the UUV. If the target goes out of range of the UUV's sensors, the UUV attempts to reaquire it. After a specified amount of time, the UUV goes back into serch mode if the target has not been reaquired. Otherwise, if the target is reaquired or if it has maneuvered, the UUV will reenter the BO-TMA mode. If the UUV determines that it has been counterdetected, it will abort the mission, shutting down to minimal power for a certain period of time and wait for a retrieval [19]. This prevents the contact from following the UUV back to its home base. If the contact has left the UUV's operating area, the UUV will report the aquired course, speed and position information to its home platform and return to its search mode. The home platform is the platform from which the UUV is launched, which could be a ship or a shore station. The UUV can report the information through a variety of means. Some of these means include using an antennae, or through underwater communication to another UUV or communication buoy. In addition, the UUV can monitor its power availability. If it does not have sufficient power, it will return to its home base to recharge before completing another mission.

3.2 Maneuver scenarios

The development of the guidance logic begins with examining the effectiveness of various maneuvers. An observer maneuver is defined as a course change at a constant speed for this thesis. These design scenarios vary both the target course and the observer maneuvers. The target course varies between 0 degrees, 15 degrees and 45 degrees. The speed (8 yd/s $\approx$ 14 kts) and the initial absolute starting point (500,500)yds of the target remain constant throughout the various scenarios. The observer also has a constant speed throughout the experiments at a value of 6 yd/s ($\approx$ 10 kts). The initial $\hat{y}$ state vector is a transformation of the absolute cartesian states of the observer and target with some added noise. The initial covariance P_0 is constant throughout the trials and is given by [1]:

$$\overline{P_0} = \begin{bmatrix} 1 \times 10^{-3} rad/s & 0 & 0 & 0 \\ 0 & 1 \times 10^{-3} s^{-1} & 0 & 0 \\ 0 & 0 & 1 \times 10^{-3} rad & 0 \\ 0 & 0 & 0 & 1 \times 10^{-7} yd^{-1} \end{bmatrix}. \quad (3.1)$$

Ten trials are run within each set-up to allow for the variation in the initial estimate quality. The trials run for 1200 sec each.

For the most part, the observer performs two maneuvers. The only exception is having the observer begin with a course moving away from the target and performing a 180 degree turn, then performing the normal two maneuvers. The different scenarios include the observer moving away from the target (Fig 3.2 :A_2), moving towards the target (Fig 3.2 :E_3), long range detection (Fig 3.2 :C_3) and short range detection (Fig 3.2 :D_1). The specific parameters of each experiment are presented in Table 3.1.

Within each trial, the observer's trajectory is plotted along with the target's actual

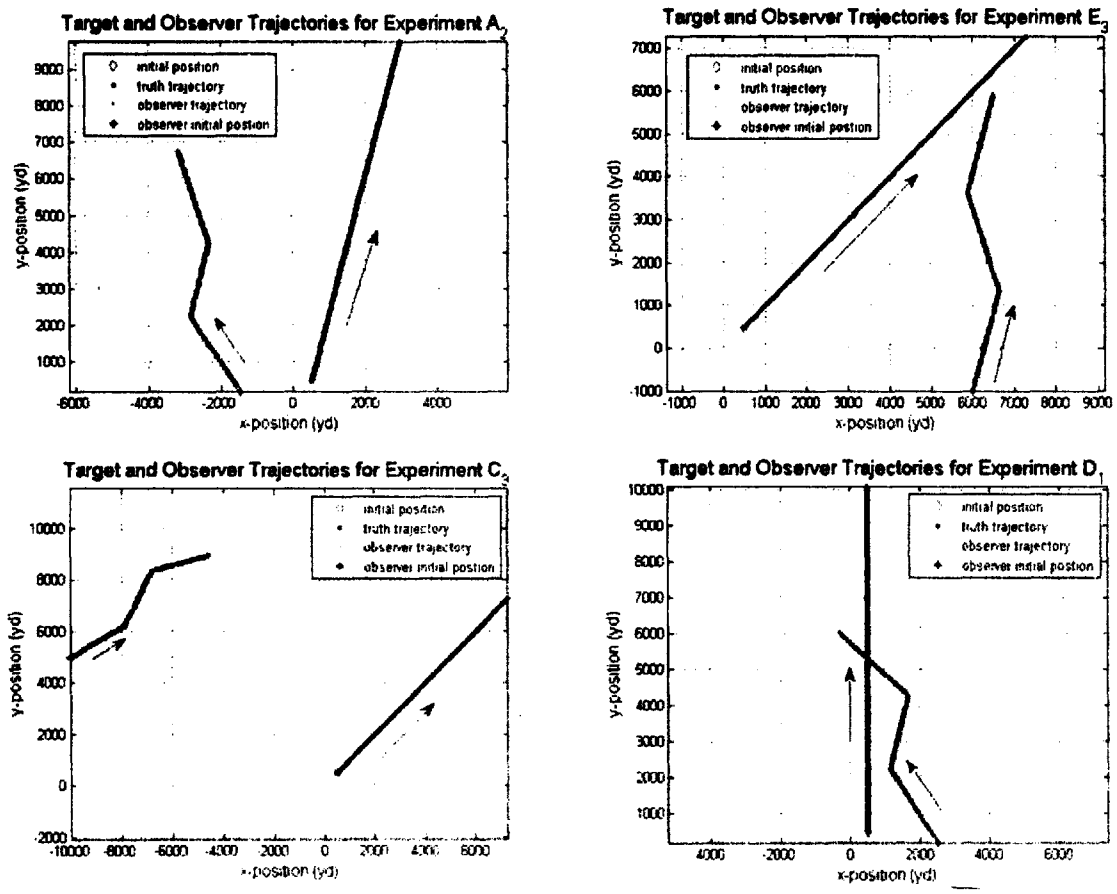

Figure 3.2: Sample Target Observer Trajectories

Experiment	Target Course (rad)	Observer Initial Position (yds,yds)	Observer Initial Course (rad)	Course Change		
				Turn 1 (rad)	Turn 2 (rad)	Turn 3 (rad)
A_1	0	(2500,200)	$3\pi/16$	$\pi/6$	$-\pi/4$	0
B_1	0	(2500,200)	$3\pi/16$	$-\pi/6$	$\pi/4$	0
C_1	0	(2500,200)	$3\pi/16$	$-5\pi/12$	$\pi/3$	0
D_1	0	(2500,200)	$-3\pi/16$	$\pi/4$	$-\pi/3$	0
E_1	0	(-1500,200)	$-3\pi/16$	$\pi/4$	$-\pi/6$	0
A_2	$\pi/12$	(-1500,200)	$-3\pi/16$	$\pi/4$	$-\pi/6$	0
B_2	$\pi/12$	(-1500,200)	0	$\pi/4$	$-\pi/6$	0
C_2	$\pi/12$	(2700,200)	$\pi/4$	$-3\pi/8$	$\pi/3$	0
D_2	$\pi/12$	(2700,200)	$3\pi/16$	$\pi/6$	$-7\pi/16$	0
E_2	$\pi/12$	(2700,200)	$3\pi/4$	$-\pi$	$\pi/6$	$-\pi/3$
A_3	$\pi/4$	(200,2500)	$\pi/12$	$\pi/3$	$-2\pi/9$	0
B_3	$\pi/4$	(-1500,200)	$\pi/16$	$\pi/4$	$-\pi/3$	0
C_3	$\pi/4$	(-10000,5000)	$\pi/3$	$-\pi/6$	$\pi/4$	0
D_3	$\pi/4$	(6000,-1000)	$-\pi/6$	$\pi/2$	$-\pi/4$	0
E_3	$\pi/4$	(6000,-1000)	$\pi/12$	$-\pi/6$	$\pi/6$	0

Table 3.1: Observer-Target Geometries

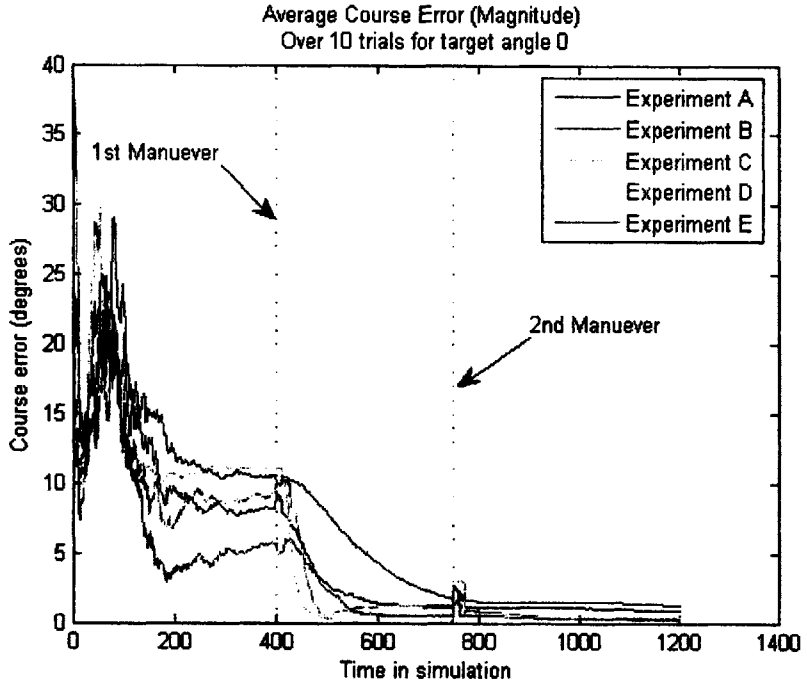

Figure 3.3: Course Error results for the set of experiments that include a target course of 0 degrees

and estimated trajectories. This is one of the areas in which the effectiveness of the maneuver is determined. Using the different parameters, various aspects and effects of the maneuvers are analyzed both qualitatively and quantitatively. For a purely qualitative analysis, the visual results of the estimated and actual trajectories are used.

For each trial and each experiment, the initial guess of the y state vector is varied from truth by a random number. The initial visualization of the results allows for a basic analysis of the effectiveness of the maneuver. The estimation often goes from having erratic behavior to a bit more consistent behavior after the first maneuver is performed (as expected). Even in cases where there are large initial errors, the maneuver brings the estimation closer to the actual course of the target.

In addition to a qualitative analysis, a quantitative analysis is performed. This quantitative analysis takes the average of the ten trials for each experiment. The initial estimatation error varies over the trials due to the random error that was added to the actual value of the state vector. Three different metrics are evaluated in each run: the error in the course estimation, the error in the speed estimation and the error in the range estimation. The calculation of the averages uses the absolute values of the errors, since the magnitude of the error provided more information than the sign of the error. An example of the results can be seen in Figures 3.3, 3.4 and 3.5.

These figures also plot the time of the maneuvers. In each of the metrics, the maneuver has an effect on the results. In both the course and speed, the error estimate levels out prior to the maneuver to a steady error. However, after the maneuver, the

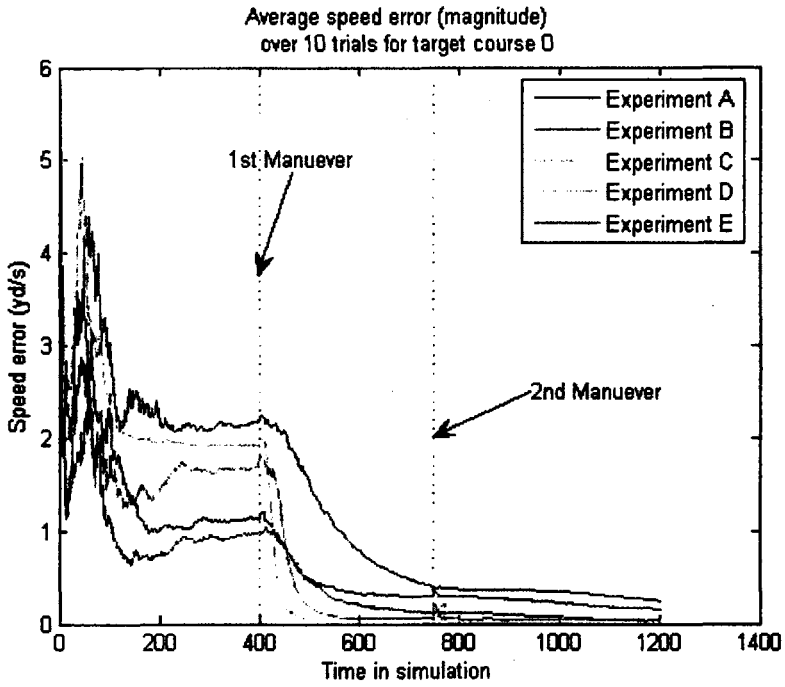

Figure 3.4: Speed Error results for the set of experiments that include a target course of 0 degrees

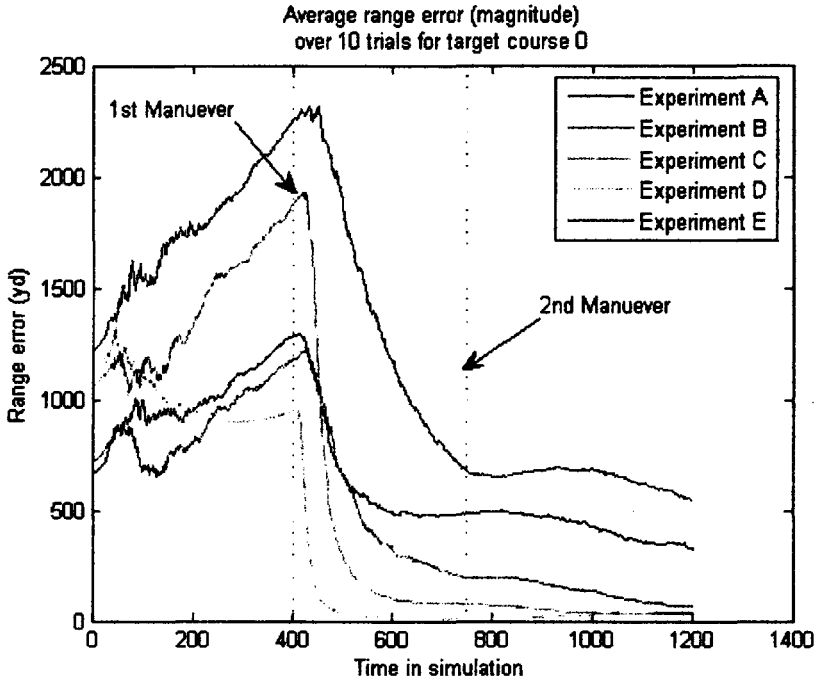

Figure 3.5: Range Error results for the set of experiments that include a target course of 0 degrees

error decreases in all three metrics. In general, the range error tends to rise prior to the observer's maneuver. The only exception in these 5 experiments is experiment D. In this case, the range error initially decreases rather than increases, due to the fact that its initial course is directed towards the target rather than away from it. The general rise in range error is the expected result since the state that includes the range is unobservable prior to a maneuver. All five of the experiments result in a decrease in the error after the first maneuver, however the steepness of that decrease varies. The quicker the drop, the more effective the maneuver. This is true within all three metrics. As can be seen in Figures 3.3, 3.4 and 3.5, experiments C and D have the most significant drops in error after the maneuver. They also have the smallest errors at the end of the run. Since these results look at the averages over ten trials, some of the large errors that occur in individual trials are smoothed out.

An observation from these experiments is that the observer's motion should generally be *towards* the target. The results of these experiments confirm the generalized rules for optimal observer maneuvers found in the literature [24]. In general, one wants to find a balance between

- increasing the bearing rate and
- decreasing the range [4].

The maneuvers that did better tend more towards the target than away from the target. Another observation from these experiments is that the initial estimate needed to be tweaked a bit. The initial estimate is based on the actual state values with some random error added to it. The issue develops for the long range scenarios since the error is added into the y state vector. In this state vector, one of the states is the reciprocal of range. For long range scenarios, the same error creates a much greater initial error since the magnitude of the error added to the state was greater than that of the state itself. In order to overcome this in the final runs, the error is added to the x state vector prior to it being transformed into y space. This change is also consistent with the scenario in which the x state vector is the information given to the UUV by the sensor network that has cued it. It is assumed that there is an initial error in the information that passed to the UUV, rather than perfect information.

3.3 Guidance logic

The guidance logic takes various factors into account. The variables that are fed into the logic include the observer's current state, the target's estimated state, the estimated y state vector, the detection of the target, the current observer course command, the future course commands, the length of an individual leg of the maneuver and the current BO-TMA command. The main output is the course command for the observer.

The first part of the guidance logic calculates a good intercept course based on the relative positions of the target and observer as well as the target's estimated course. The goal of this logic is to calculate a course that will allow the observer to come

within range of the target. In order to do so, the observer's course must be in the direction of a point ahead of the target's current position. In order to achieve this point, the command course is chosen to be either perpindicular to, 45 degrees off of or 15 degrees off of the target's estimated course based on the relative positions of the observer and target. If the observer course is close to parallel to the estimated bearing between it and the target, its course remains constant. Otherwise, the observer turns towards the target's course.

Once the target is within range of the observer, the guidance calculates the BOTMA maneuver. The basis of this maneuver are the guidelines presented in the literature that have been verified within this thesis. The maneuvers follow a basic Z pattern as described in Passerieux and Van Cappel's work [24]. The guidance logic calculates the two different courses the observer needs to take. The general direction of the maneuver is always towards the target. In each of the following cases, the third leg of the maneuver is the same as the first leg of the maneuver.

- If the observer's course is within 15 degrees of the target's estimated course
  - The first leg of the maneuver is the observer's current course
  - The second leg of the maneuver turns towards the target with a course that is 30 degrees off of the target's estimated course
- If the observer's course is close to being the reciprocal[1] of the target's estimated course
  - The first leg of the maneuver is the target's estimated course
  - The second leg of the maneuver turns towards the target with a course that is 30 degrees off of the target's estimated course
- If the observer's course is towards the target
  - The first leg of the maneuver is the observer's current course
  - The second leg of the maneuver is the target's estimated course
- If the observer's course is away from the target
  - The first leg of the maneuver is the target's estimated course
  - The second leg of the maneuver turns towards the target with a course that is 30 degrees off of the target's estimated course

The guidance algorithm allows the maneuver to complete, even if the target is out of range of the observer. Once the maneuver is complete, the observer will either come to a course parallel to the target's estimate or it will turn around, indicating that the target has moved outside the range of the observer. However, this does not happen immediately but rather after a specified amount of time has elapsed.

[1] A bearing 180 degrees from the other

The guidance logic also keeps track of the history of the target state estimations. The history provides the metric to determine whether or not another maneuver is required. One of the basic assumptions for this problem is that the target has a constant course and speed. Within the estimation, small variations are expected. However, if there is a large jump within either the course or the speed history, a new maneuver is required to maintain the integrity of the estimation. Once this is determined, the guidance algorithm will calculated another set of maneuvers.

If the target leaves the range of the observer's sensors, the observer continues on its current course for a specified time in order to try to reaquire the target. If the observer does not reaquire the target, it turns away from the last known position of the target and returns to its home base. In the simulation, this is represented by a 180 degree turn.

The guidance logic is incorporated into the main control of the UUV. The next chapter will explore the environmental model and simulation set-up.

Chapter 4

Simulation and Environment Models

This chapter explores the environmental and the simulation models. The underwater environment is a tough environment to model. This chapter presents the various simplifications and assumptions made in the final simulations. After exploring the sensor detection radius and environment, this chapter will present the set up for the various trials used to test the guidance algorithm.

4.1 Detection Algorithm

The detection algorithm determines whether or not the target is within the range of the passive sonar. If the range of the sonar extends past the location of the target, then the target is detected. A sonar range algorithm is used in conjunction with the detection algorithm.

The range in which a target can be detected depends on various factors and parameters. For passive sonar, these factors are the target source level (SL), the ambient and self-noise level (NL), the transmission loss (TL), the detection threshold (DT) and the receiving directivity index (DI) [28, 27]. These parameters are combined in the passive sonar equation:

$$SL - TL - NL + DI \geq DT, \tag{4.1}$$

expressed in dB. The range at which a target is likely to be detected can be estimated by solving for the transmission loss at a specific detection threshold:

$$TL = 20\log_{10} r_0 + 10\log_{10}\frac{r}{r_0} + \alpha\left(r \times 10^{-3}\right) \tag{4.2}$$

where r_0 is the transition range between spherical and cylindrical spreading and α is the attenuation coefficient. In order to simplify the calculations, the transmission loss due to attenuation is assumed to be very small. It is also assumed that the transmission loss is due to spherical spreading and the effects of cylindrical spreading

are ignored. This results in

$$TL \approx 10\log_{10} r \tag{4.3}$$

being the function used to calculate the range of the sonar. This relation is a simplified version of a more detailed model and does not take into account all of the aspects of the environment. However, the purpose of this exercise is to have a way to model the range of the sonar in the scenario with some basis in reality rather than picking a number out of thin air.

The detection threshold is the point at which the system determines that there is a contact. This threshold is based on the detection index desired for the sonar, as well as the bandwidth and integration time of the sonar. The detection index is pulled off of a chart based on the desired probability of detection, $p(D)$, and probability of a false alarm, $p(FA)$:

$$DT = 5\log_{10}\left(\frac{d}{T\Delta f}\right) \tag{4.4}$$

where d is the detection index, T is the integration time and δf is the bandwidth frequency of the sensor.

The directivity index, detection threshold and the self-noise are all parameters based on the sonar equipment. The directivity index depends on the type of array used as well as the frequency of the sound wave. There are many different estimations of the directivity index, depending on the shape of the array. For this thesis, the sonar was assumed to be a conformal array, with a DI of 19.54 dB at broadside [11]. For the purpose of these calculations, the directivity index was assumed to be constant thoughout the entire scenario. The transmission loss and the ambient noise level depend on the environment that the observer is in. The noise level in the passive sonar equation includes the self-noise and the ambient noise of the environment:

$$NL_{amb} = NL_{ss} \oplus NL_{ship} \tag{4.5}$$

$$NL_{tot} = NL_{amb} \oplus NL_{self} \tag{4.6}$$

where $\oplus$ represents the power sum of two decibel quantities:

$$L_1 \oplus L_2 = 10\log_{10}\left(10^{\frac{L_1}{10}} + 10^{\frac{L_2}{10}}\right). \tag{4.7}$$

The source level is the level of noise radiated by the target [18, 27, 28]. Of these parameters, only the transmission loss is unknown. The sonar parameters are modeled based on known literature. Within this thesis, two environments will be modeled through the use of varying the ambient noise level for different conditions. The source level of the target can also be modeled for various targets. This variation is important because it allows for the effectiveness of the algorithm to be evaluated in different situations.

The model of the source level of the target used and modified old data from World War II era submarines [18, 28]. It is assumed that all current data is classified, but that the presented model can easily be adjusted for proper parameters.

Once the sonar range algorithm calculates the detection range, the detection algo-

rithm can determine whether or not the UUV can "hear" the target. This algorithm is used both in initiating the bearings only tracking as well as maintaining the track of the target.

4.2 Environment

Target motion analysis and target tracking are common activities in blue water environments. Blue water environments are also known as open ocean or those waters that lay beyond the coastal regions of the earth [23]. A key benefit of using UUVs is to perform this mission within a littoral area. The littoral area is that area that is closest to shore (within 600 feet of the shoreline) [23]. The UUV would be able to penetrate closer to harbors and choke points than would a manned sub, effectively becoming a force multiplier. The effects of the environment are simulated within the passive sonar equation in the detection algorithm.

For the purpose of this thesis, two different scenarios are created. Their specific parameters are presented in Table 4.1. Both occur in shallow water environments. The two aspects of the ambient noise are due to shipping and to the sea state. The two different scenarios represent a typical day (refered to as the nominal case) and a worse case scenario type of day. For the typical day, the shipping is assumed to be heavy since the UUV would be acting either just outside a harbor or a choke point. The sea state is assumed to be 1, with a wind speed of four to six knots. For the worst case scenario, the sea state is assumed to be 6, the highest sea state with wind speeds of 28 to 33 knots. Since it is a very heavy sea state, the shipping levels are assumed to be moderate.

Wenz curves are used in order to convert this information into the decibel form that is required for the passive sonar equation [18, 27, 28]. Figure 4.1 is a simplified version of the Wenz curves that was used to determine the noise levels due to shipping and sea state. The value is found at the intersection of the shipping or sea state with the center frequency of the bandwidth. The center frequency is found by taking the geometric mean of the two end frequencies of the bandwidth.

Parameter	Environment 1: Nominal Case	Environment 2: Worst Case
Self noise (NL_{self})	50 dB	50 dB
Source level (SL)	110 dB	110 dB
p(D)	.90	.90
p(FA)	.002	.002
Bandwidth (Δf)	400 Hz	400 Hz
Integration time (T)	20 ms	20 ms
Sea state	1	6
NL_{ss}	81 dB	99 dB
Shipping	heavy	moderate
NL_{ship}	93 dB	80 dB

Table 4.1: Environment Parameters

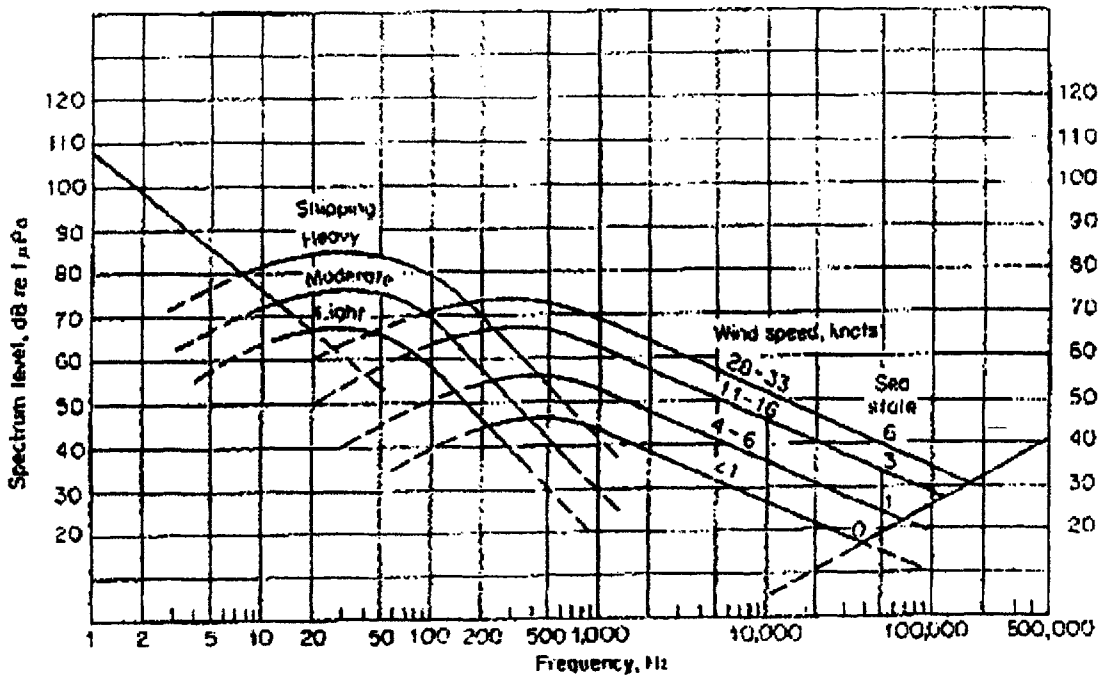

Figure 4.1: Simplified Wenz Curve [27]

4.3 Vehicle capabilities

This thesis contains two separate vehicles, the UUV, or observer, and the contact, or target. In order to simplify the estimation process, the target's motion is assumed to have a constant velocity. In a choke point situation, this assumption is more realistic due to the restrictions to motion in most choke points. The target would not be able to make an unexpected or rapid course or speed change. Once it has left the restricted area, however, maneuvers are possible. However, within this set up, the target maintains course and speed for the entire experiment. The speed of the target is restrained by the area it is operating in.

The UUV on the other hand has the ability to manuever. The main restraint on these maneuvers is a constant turning rate of 3 degrees/s. In most cases, the UUV is slower than the target. Its unrestrained speed capability is less, but there could be situations in which the UUV is traveling faster than the target. The UUV maintains a constant speed throughout the experiments. The basic dynamic equations of both the target and observer are

$$x_t = x_{t-1} + v_{t-1}\sin(\theta_{t-1}) \tag{4.8}$$

$$y_t = y_{t-1} + v_{t-1}\cos(\theta_{t-1}) \tag{4.9}$$

$$v_t = v_{t-1} \tag{4.10}$$

$$\theta_t = \theta_{t-1}. \tag{4.11}$$

When the observer is in the middle of a maneuver the last equation alters to

$$\theta_t = \theta_{t-1} + \dot{\psi}\Delta t \tag{4.12}$$

where $\dot{\psi}$ is the turning rate.

4.4 Simulation set-up

In order to examine the effectiveness of the guidance algorithm, a number of different situations were created. The different variables are the target-observer geometry, the speed ratio and the difference between the nominal and worst case environment. Throughout all of the experiments, the observer had the same position in the center of the environment. The target's location, course and speed were varied for each of the experiments.

4.4.1 Nominal cases with geometric variations

The first set of experiments have varying geometries. The speeds of the observer and target remain constant throughout these experiments: 6 yds/s and 8 yds/s, respectively. The initial position of the observer also remains constant through all of the experiments. The target's initial position and the courses of both the target and the observer are varied throughout these experiments. Table 4.2 contains the specific values of these variables.

The five different geometries represent a variety of situations as seen in Figures 4.2, 4.3, 4.4, 4.5 and 4.6. These figures are not to scale in Cartesian space. In experiment 2, the UUV is behind the target while in experiment 5, the observer is initially on a close to reciprical course with the target. In the other three experiments, the observer is off to one side or the other of the target's projected course. They vary in the direction of the initial observer course in reference to the target's course.

4.4.2 Nominal cases with speed variations

The next set of experiments examines the effect of different target-to-observer speed ratios on the effectiveness of the guidance system. There are three different speed

Experiment	Target Initial Position (yds,yds)	Target Course (rad)	Observer Initial Course (rad)
1	(-3000,2000)	$\pi/3$	$7\pi/4$
2	(-200,-1000)	$5\pi/4$	$3\pi/2$
3	(3000,-3500)	$8\pi/5$	$3\pi/2$
4	(-2000,-1500)	$4\pi/7$	$\pi/12$
5	(-5000,-5000)	$\pi/4$	$7\pi/6$

Table 4.2: Simulation parameters for nominal case geometries

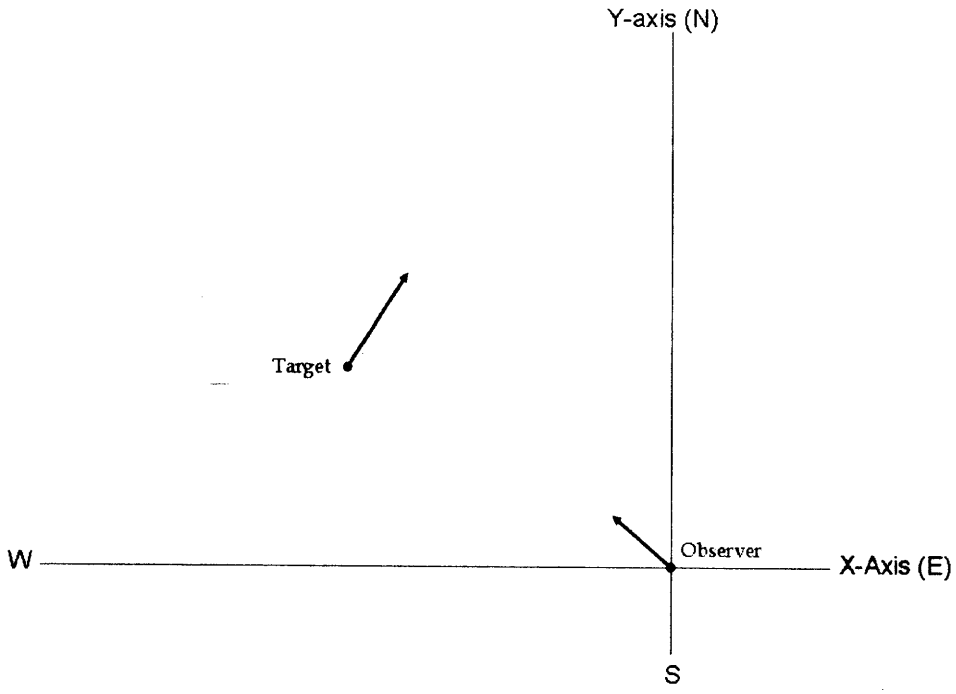

Figure 4.2: Experiment 1 Geometry

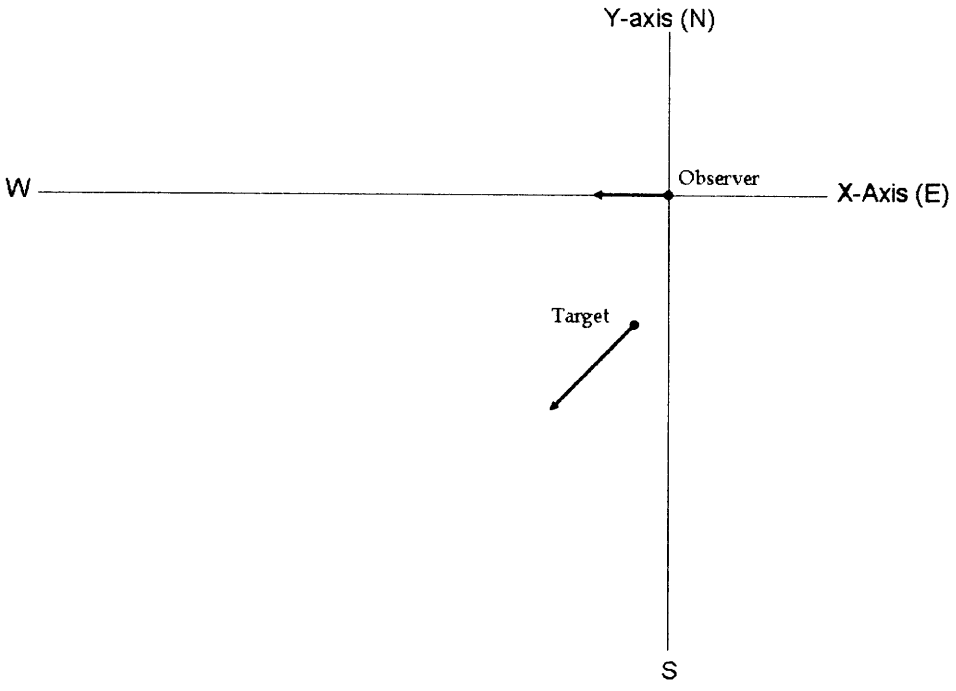

Figure 4.3: Experiment 2 Geometry

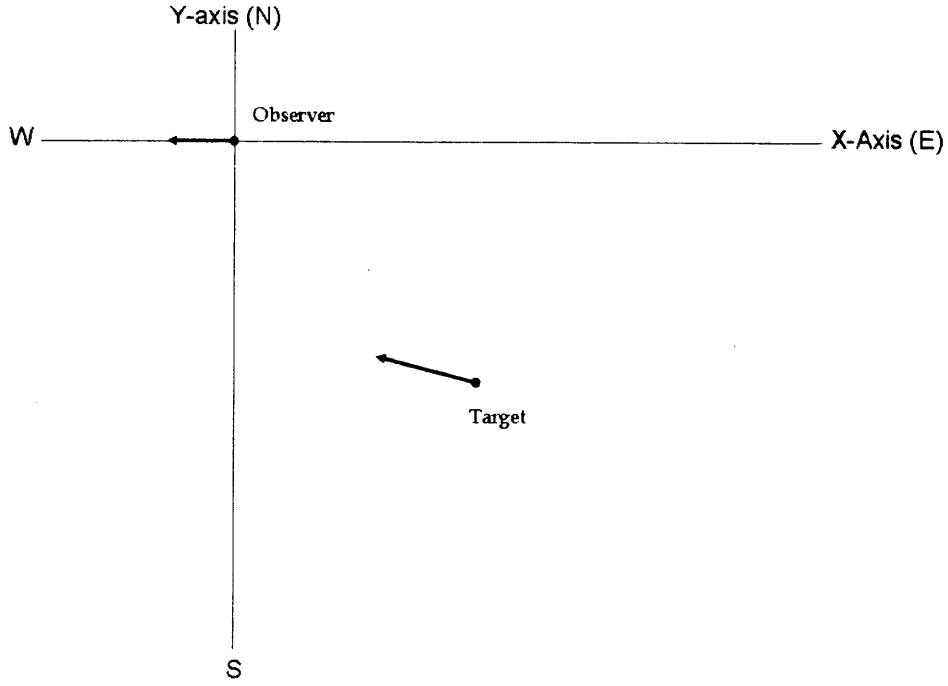

Figure 4.4: Experiment 3 Geometry

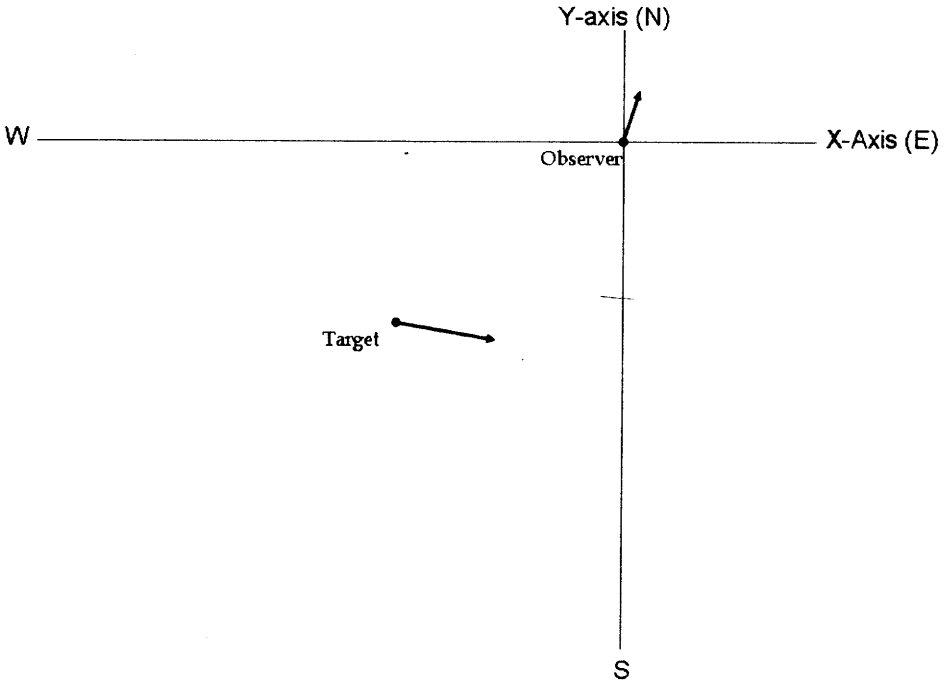

Figure 4.5: Experiment 4 Geometry

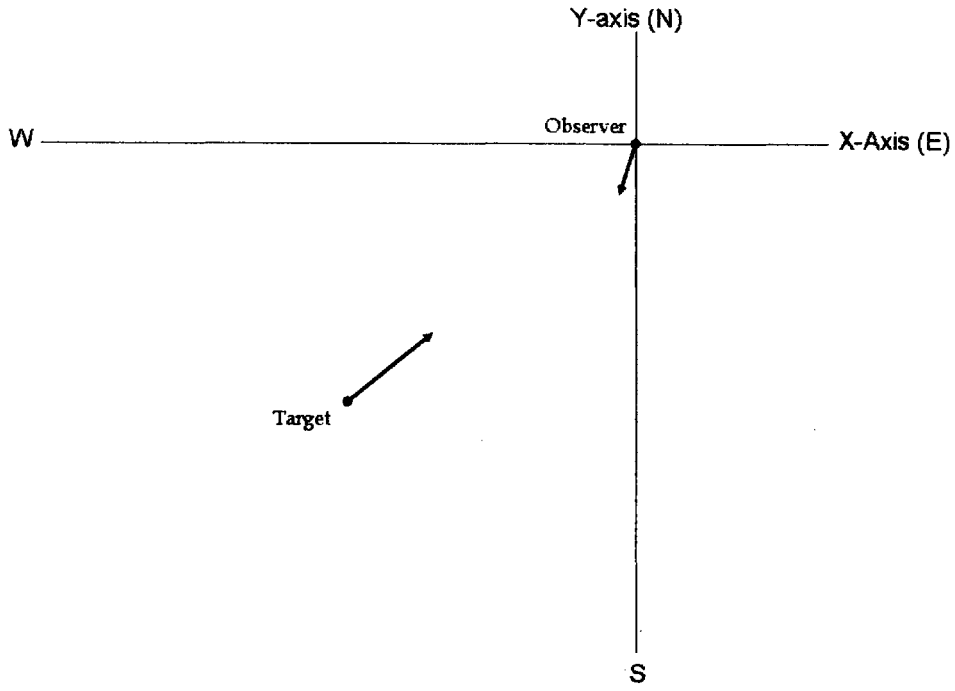

Figure 4.6: Experiment 5 Geometry

Experiment	Target Speed (yds/s)	Observer Speed (yds/s)
2	8	6
6	8	8
7	6	8

Table 4.3: Simulation parameters for nominal case speed ratios

ratios: 4:3, 1:1 and 3:4. In other words, the three different cases consist of the observer being slower than the target, the same speed as the target and faster than the target. The geometry of the situation remains constant throughout the three different situations. This geometry is the same as experiment 2 as seen in Figure 4.3. Again, the environmental set up is that of the nominal case. The actual speeds of the observer and target for each experiment is presented in Table 4.3.

4.4.3 Worst Case

In addition to the nominal cases, worst case experiments are run to examine the point in which the guidance algorithm breaks down. The first group of experiments looks at the effect of speed in this noisy environment (as described in Table 4.1). As in the speed experiment for the nominal case, the speed ratio is varied. The main differences between experiments 8, 9 and 10 and the nominal case speed experiments are the noise due to shipping and the noise due to the sea state. The geometry remains

Experiment	Target Speed (yds/s)	Observer Speed (yds/s)
8	8	6
9	8	8
10	6	8

Table 4.4: Simulation parameters for worst case speed ratios

constant for these experiments, being the same as that of experiment 2 (Figure 4.3). The actual speeds for the experiments are presented in Table 4.4.

In addition to the speed experiments, a final experiment, experiment 11, is run in the worst case environment for comparison to the nominal case. The geometry of this final experiment is the same as experiment 4 in the nominal case (Figure 4.5). The speed ratio returns to the typical 4:3 of the initial cases.

4.5 Final experimental setup

Five trials are run for each of the experiments. In order to repeat the results of each trial, a seed is used in the generation of the random numbers within the simulation. This allows the sensor noise and initial estimation error to remain random, but repeatable. The simulation time is 3600 s. The observer has a turn rate of $\pi/60$ rad/s. The length of the maneuver legs is 400 s.

The next chapter will present the results from these experiments.

Chapter 5

Experimental Results

This chapter presents the results from the four different experiments as outlined in Section 4.4. Within each set of experiments, data in both the cartesian coordinates and the modified polar coordinates will be shown. The x state space results consist of speed error, course error and range error. The y state space (modified polar) includes the bearing, bearing rate, normalized range rate and reciprocal of range. The covariance is updated within the Kalman filter, so that information is presented in the y state. The errors in the x state demonstrate the accuracy of the information that will be passed on from the observer to its home base.

5.1 Nominal Case Geometry Experiments

The first set of experiments vary the geometry within the nominal environment as shown in Table 4.2. One metric of the effectiveness of each geometry is the time at which the target moves out of the detection range of the observer. The longer the observer maintains contact with the target, the more information it can obtain. Therefore, those geometries which result in a longer time of contact can be considered more effective in gathering information. These times are presented in table 5.1.

After each trial is run, the trajectories for the observer and the target are plotted. This plot gives a visual representation of both the observer's motion and the accuracy of the estimated target motion. Figure 5.1 shows the results for the fourth

Experiment	Trial 1	Trial 2	Trial 3	Trial 4	Trial 5	Mean
1	1677 s	1709 s	1712 s	1675 s	1709 s	1696 s
2	926 s	908 s	917 s	871 s	909 s	906 s
3	2258 s	2431 s	2234 s	2023 s	2216 s	2232 s
4	1785 s	1831 s	1814 s	1915 s	1832 s	1835 s
5	2534 s	2514 s	2530 s	2480 s	2514 s	2514 s

Table 5.1: Loss of detection in the nominal case geometries. The time for each trial at which the target leaves the observer's sensor range, and the average for each experiment.

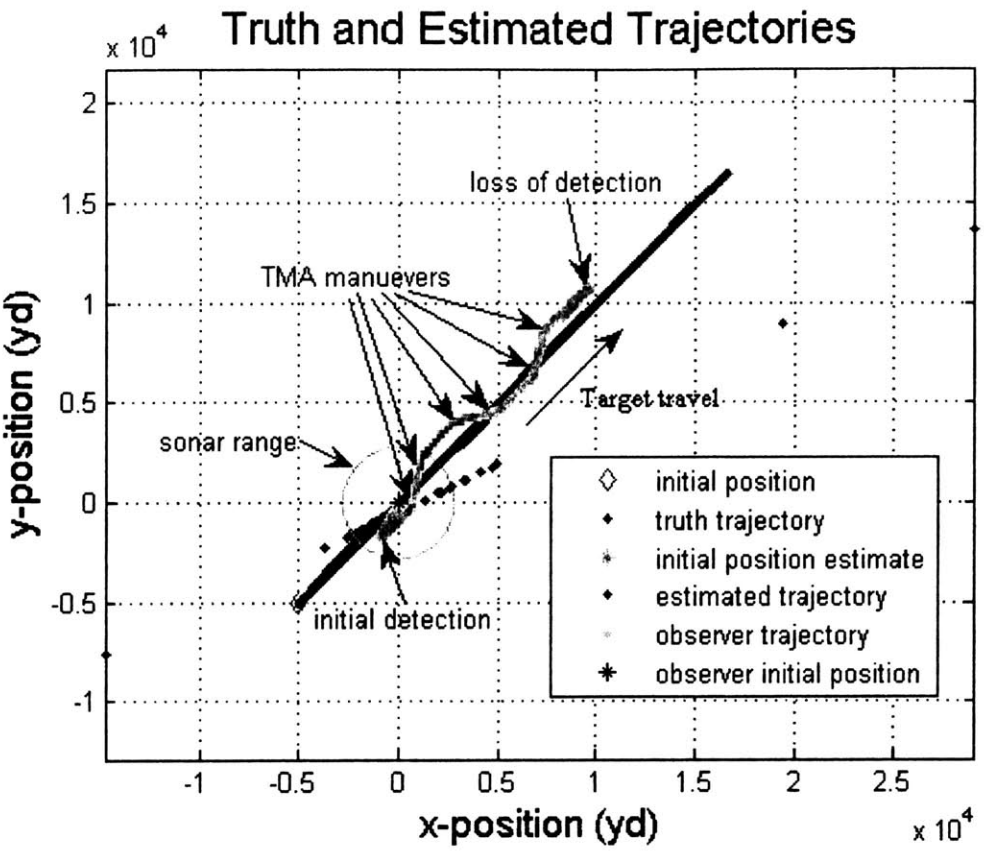

Figure 5.1: Experiment 5: Observer and Target Trajectories

trial of experiment 5. This plot contains the actual trajectory of the target, the estimated trajectory of the target and the observer's trajectory. In addition, there is a circle indicating the range of the observer's sonar at its initial position. This plot demonstrates the maneuvers that the observer has completed during the run. In this particular plot, the observer has calculated three different BO-TMA maneuvers. These maneuvers are labeled on the plot. Towards the end of the run, the observer completes a 180 degree turn (as label in Figure 5.1), which indicates that the target is no longer within range of its sensors.

The absolute time at which the target moved outside of the observer's sensor range can be determined from the plots of both the speed and course error. Once the target is out of range, the filter continues to propagate the estimate, but no longer updates it since there are no measurements. Due to the modeled dynamics of the target, its course and speed remain constant once it is out of range of the observer. In the same way, the estimated course and speed remain constant, resulting in constant position error growth. The point at which the graphs become constant is the time that the target leaves the sensing range of the observer. The jumps that can be seen in between constant values are a result of observer maneuvers after the target has left the observer's sensor range.

In addition to the trajectories, the range, course and bearing errors are plotted

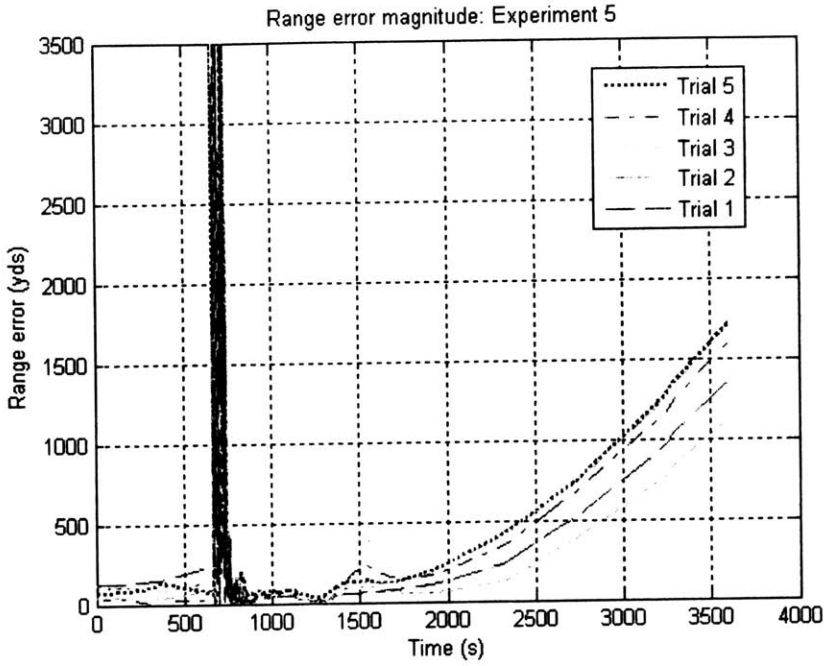

Figure 5.2: Range Error Plot

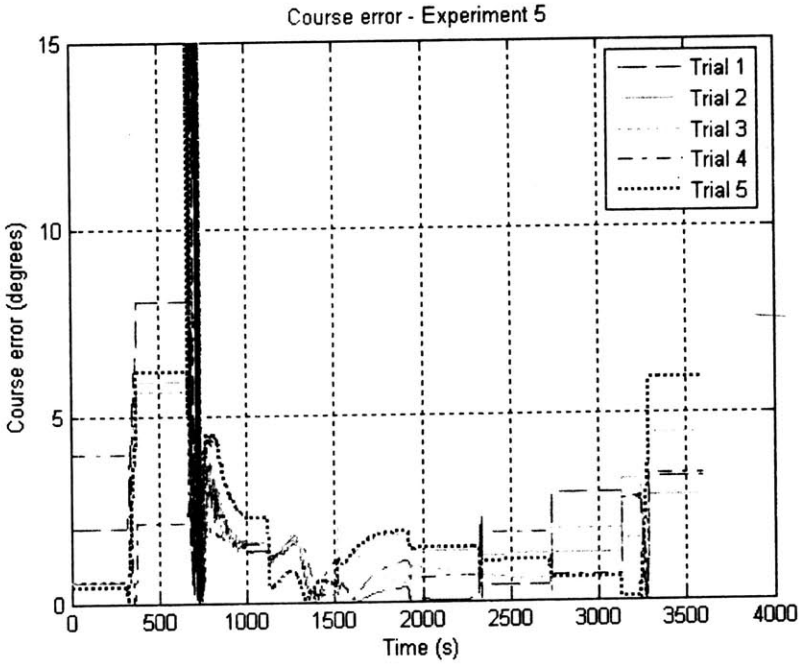

Figure 5.3: Course Error Plot

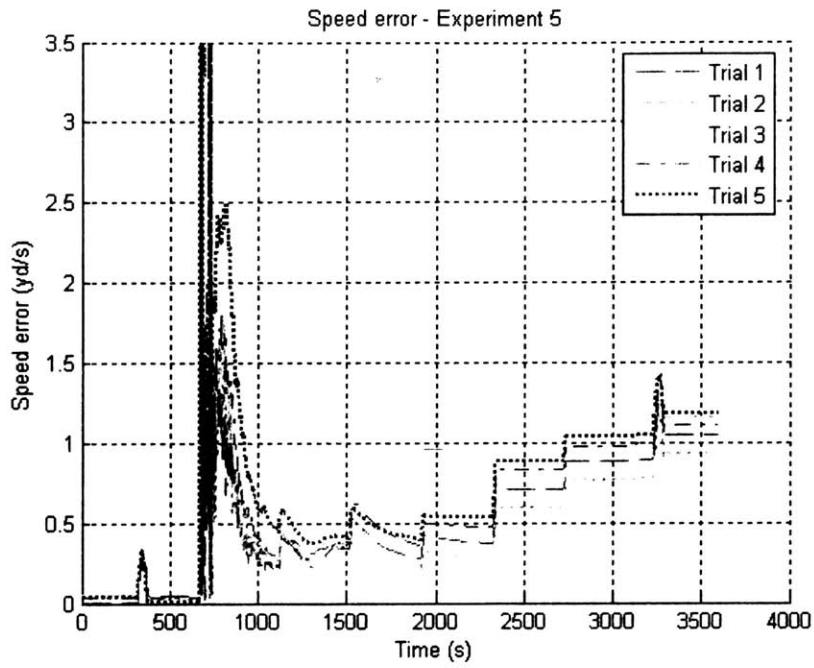

Figure 5.4: Speed Error Plot

for each trial of the experiment. Figures 5.2, 5.3 and 5.4 include the x state errors for experiment 5. In this experiment, each trial has a very similar result, with offset due to the random values. Some of the other experiments, on the other hand, have a trial or two that do not quite follow a similar pattern in the plotted errors. Similar plots are created for each of the other experiments.

Most of the experiments in this set have the large jump in the errors that can be seen in Figures 5.2, 5.3 and 5.4. This jump occurs when the filter begins to update its estimations based on the sensor measurements. The points can be seen in Figure 5.1 that result in these large errors. The range is unobservable prior to the first course change of the BO-TMA maneuver. These estimated positions of the target also demonstrate the bearing ambiguity prior to the maneuver. The bearing ambiguity occurs when the bearing measurement crosses from 2π to 0 radians. Once the maneuver occurs, the estimation smooths out. The only experiment that does not have these large errors at the beginning of the run is experiment 2. This is due to the geometry of the experiment, where the observer is coming from behind the target, and there is a smaller range than the other 4 experiments.

The observer reports the target information obtained immediately prior to the point in which the contact goes out of range. Table 5.2 includes the error in the reported information. These results present a snapshot of the entire error plots. The mean range error is about 18.5 percent of true range in experiment 1, 20.4 percent of true range in experiment 2, 42.3 percent of true range in experiment 3, 14.8 percent of true range in experiment 4 and 16.1 percent in experiment 5. From the errors in the reported information, experiment 4 has one the lowest values in each of the three different metrics. The large range errors in experiment 3 are directly related to its

	Range Errors (yds)					
Experiment	Trial 1	Trial 2	Trial 3	Trial 4	Trial 5	Mean
1	862	513	463	261	480	516
2	603	536	623	404	674	568
3	162	4304	43	1078	319	1181
4	102	351	514	697	401	413
5	385	558	255	471	567	447
	Course Errors (rad)					
Experiment	Trial 1	Trial 2	Trial 3	Trial 4	Trial 5	Mean
1	0.0954	0.0419	0.0386	0.00346	0.0356	0.0430
2	0.0260	0.0336	0.0318	0.0381	0.0348	0.0329
3	0.0202	0.0415	0.00536	0.0215	0.0284	0.0234
4	0.0517	0.0234	0.00159	0.0126	0.0166	0.0212
5	0.00717	0.0216	0.0105	0.0320	0.0188	0.0180
	Speed Errors (yd/s)					
Experiment	Trial 1	Trial 2	Trial 3	Trial 4	Trial 5	Mean
1	0.743	0.761	0.718	0.521	0.726	0.694
2	0.885	0.797	0.777	0.617	0.399	0.695
3	0.432	2.979	0.403	1.213	0.626	1.131
4	0.443	0.622	0.758	0.538	0.645	0.601
5	0.711	0.882	0.603	0.831	0.888	0.783

Table 5.2: Errors in reported information at the time of contact loss for the nominal case geometries

large speed errors. This experiment had both trials that performed poorly and one (trial 3) that performed very well. Experiment 5 was the most effective in measuring the course of the target and consistant in its other measurements.

The other set of data for these experiments consists of the elements from the y state vector. The errors in these elements were plotted along with the corresponding filter covariances. These plots provide a picture of how the filter is working. Figures 5.5, 5.6, 5.7 and 5.8 contain the original and a version zoomed around the x-axis for experiment 4. These are the results of the second trial of experiment 4.

In figures 5.6 and 5.8 the effect of the observer's maneuvers on the covariance can be seen. There is always some sort of dip or growth when the observer changes its course. The errors in the y state vector are typically small for all of the experiments. Most of the variations can not be seen until the plot is tightened around the x-axis. As can be seen in the figures, the error does not always stay within the bounds of the covariance. For a perfectly tuned filter, the error is expected to be out of the covariance bounds about 32 percent of the time. However, the error is still quite small in most cases. The growth in the bearing error that can be seen in Figure 5.6 occurs after the observer has lost contact with the target and is no longer receiving bearing measurements. Similar growths can be seen in the plots of the other experiments.

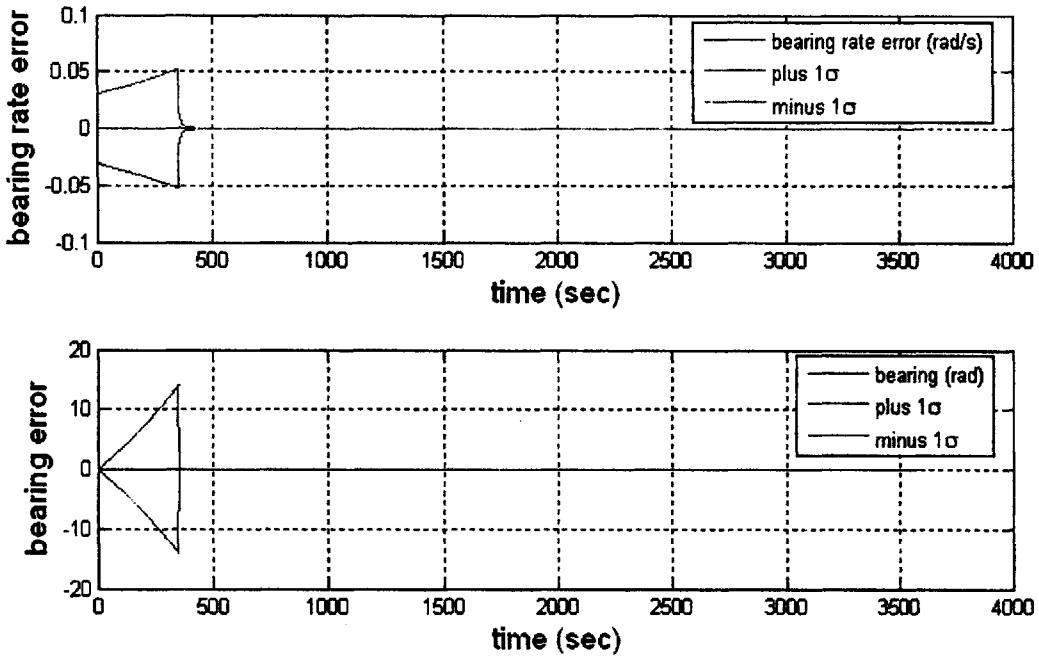

Figure 5.5: Bearing and Bearing Rate Errors and Covariance for Experiment 4.

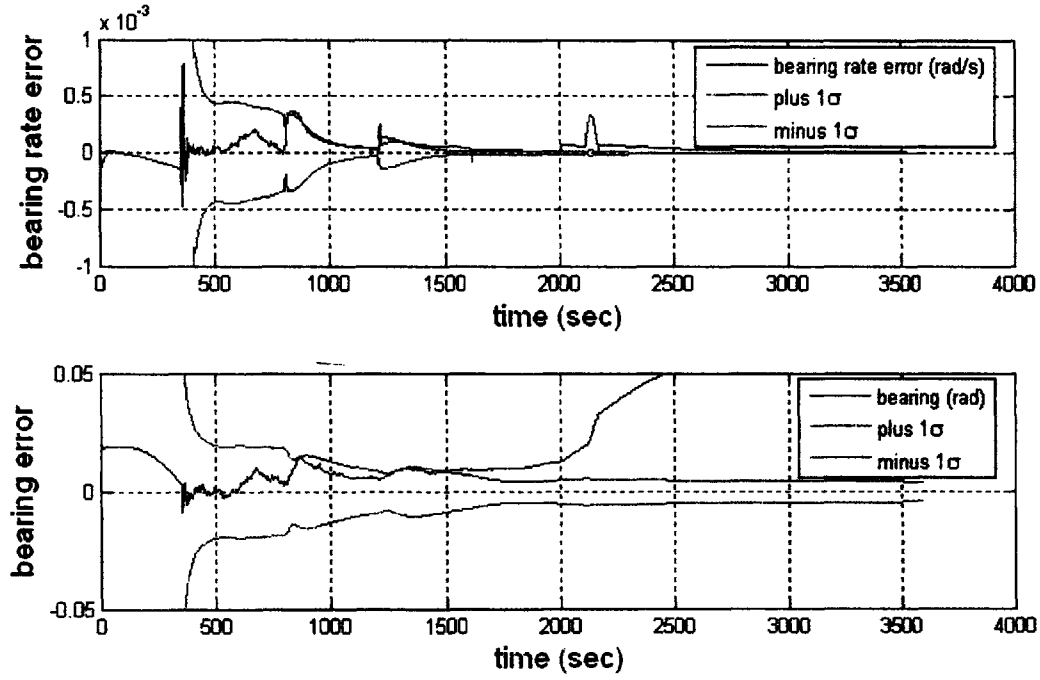

Figure 5.6: Bearing and Bearing Rate Errors and Covariance Zoomed in Around the x-axis for Experiment 4.

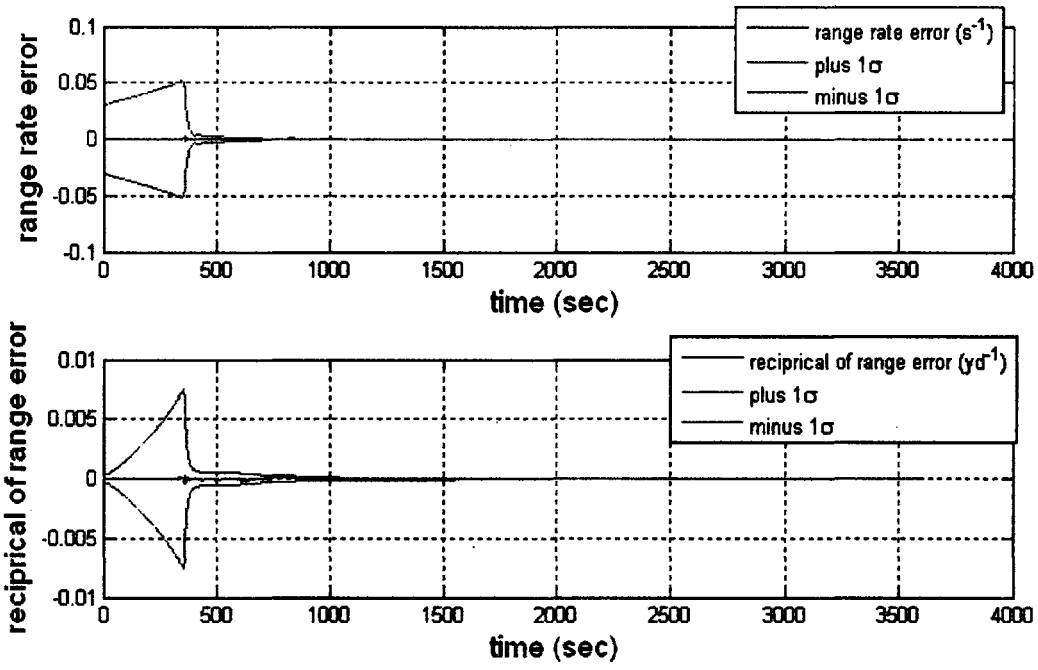

Figure 5.7: Range Rate and Reciprocal of Range Errors and Covariance for Experiment 4.

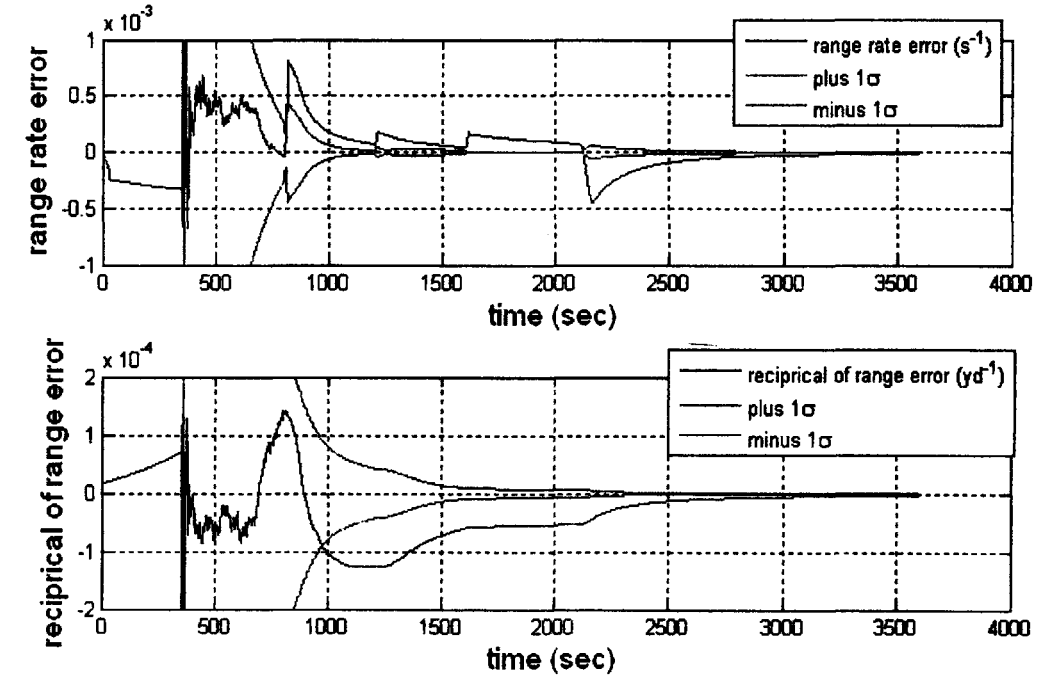

Figure 5.8: Range Rate and Reciprocal of Range Errors and Covariance Zoomed in Around the x-axis for Experiment 4.

	Bearing Rate Errors (rad/s)($\times 10^{-5}$) **Bearing Rate Covariance (σ)($\times 10^{-5}$)**					
Experiment	Trial 1	Trial 2	Trial 3	Trial 4	Trial 5	Mean
1	22.7	-5.09	-4.60	-8.48	-5.58	9.29
	2.64	2.29	2.29	2.15	2.31	2.33
2	-1.57	-1.10	-1.74	0.208	-2.12	1.35
	14.3	17.5	16.0	28.9	18.1	19.0
3	-12.8	228.0	-0.776	-1.24	-2.23	49.0
	0.267	0.353	0.783	1.78	0.933	0.823
4	14.9	6.88	2.22	2.87	5.08	6.39
	1.66	1.50	1.33	0.549	1.44	1.30
5	-13.3	-10.2	-6.90	-6.63	-10.9	9.59
	0.818	0.849	0.843	0.980	0.867	0.871
	Bearing Errors (rad) **Bearing Covariance (σ)**					
Experiment	Trial 1	Trial 2	Trial 3	Trial 4	Trial 5	Mean
1	0.0242	-0.0061	-0.0046	-0.0190	-0.0085	0.0125
	0.0091	0.0085	0.0085	0.0080	0.0085	0.0085
2	-0.0021	-0.0012	-0.0021	-0.0017	-0.0038	0.0022
	0.0149	0.0158	0.0153	0.0172	0.0158	0.0158
3	-0.0134	0.7773	-0.0571	-0.0310	-0.0384	0.1843
	0.0036	0.0028	0.0034	0.0056	0.0036	0.0038
4	0.0344	0.0194	0.0097	0.0110	0.0171	0.0183
	0.0045	0.0047	0.0045	0.0051	0.0045	0.0047
5	-0.0053	-0.0223	0.0181	-0.0087	-0.0248	0.0158
	0.0031	0.0030	0.0032	0.0031	0.0031	0.0031

Table 5.3: Bearing and Bearing Rate Errors and Covariances for Nominal Case Geometries

Tables 5.3 and 5.4 presents the y state errors and covariances at the time at which the observer loses contact with the target.

Again, Tables 5.3 and 5.4 provide a snapshot of the effectiveness of the filter at the time the observer loses contact with the target. Experiment 2 is the only experiment in which the errors typically occur within the bounds of the covariance for every metric except the normalized range rate. The errors of the other experiments are typically out of the covariance bounds at the time of contact loss. However, there are various degrees of severity. For example, the mean error for experiment 3 is two orders of magnitude greater than the mean covariance. However, the specific errors for trial 3 of experiment 3 fall much closer to if not within the bounds of the covariance. This confirms the results from the x state errors that experiment 3's third trial performed well. The results of the y state errors present another picture that confirms the picture painted by the x state results.

	Normalized Range Rate Errors (1/s)($\times 10^{-5}$) **Normalized Range Rate Covariance (σ)($\times 10^{-5}$)**					
Experiment	Trial 1	Trial 2	Trial 3	Trial 4	Trial 5	Mean
1	14.0	6.55	7.02	6.16	6.41	8.03
	2.06	1.51	1.54	1.43	1.47	1.60
2	12.2	10.9	8.14	8.57	-4.48	8.85
	4.18	4.14	4.93	5.32	8.15	5.34
3	1.49	23.4	6.90	13.9	5.19	10.2
	0.504	0.369	0.969	1.14	1.08	0.812
4	9.61	10.9	11.6	2.45	10.6	9.03
	0.436	0.256	0.299	0.293	0.263	0.309
5	11.2	7.24	13.8	9.46	6.98	9.74
	0.355	0.370	0.401	0.430	0.373	0.386
	Reciprocal of Range Errors (1/yd)($\times 10^{-5}$) **Reciprocal of Range Covariance (σ)($\times 10^{-5}$)**					
Experiment	Trial 1	Trial 2	Trial 3	Trial 4	Trial 5	Mean
1	16.1	-5.58	-5.11	-3.07	-5.27	7.02
	1.14	1.29	1.29	1.53	1.29	1.31
2	-6.38	-5.79	-6.56	-4.55	-6.99	6.05
	9.12	11.0	10.1	17.9	11.3	11.9
3	-1.97	-101.8	-0.542	-10.0	-3.69	23.6
	0.353	0.104	0.573	1.08	0.6443	0.551
4	-1.27	-4.01	-5.58	-7.18	-4.51	4.51
	0.882	0.827	0.768	3.16	0.817	1.29
5	-4.37	-5.98	-3.01	-5.19	-6.07	4.92
	0.240	0.233	0.257	0.283	0.237	0.250

Table 5.4: Normalized Range Rate and Reciprocal of Range Errors and Covariances for Nominal Case Geometries

5.2 Nominal Case Speed Experiments

The next set of experiments varied the speed ratio between the target and the observer. The parameters of these experiments are presented in Table 4.3. As previously stated, each experiment uses the geometry from experiment 2 in the previous set of experiments. In this situation, the observer is following the target. Table 5.5 presents the time at which the target leaves the sensor range of the observer. Somewhat counterintuitively, the situation in which the target and the observer travel at the same speeds maintains the longest contact. In fact, in one trial, the target is detected by the observer for the entire run. When the target is slower than the observer, the observer moves itself out of range of the target due to its greater speed. Since the observer can be considered ahead of the target in this case, it is possible for it to reaquire the target when it turns around and heads back towards its origin (in effect heading back towards the target). This occurs in the first and fourth trials in experiment 7.

As in the previous set of experiments, the trajectories are plotted after each run. Figure 5.9 represents a typical run in the speed ratio experiments. In this particular case, the target and observer have the same speed. Once again, in this particular run, the BO-TMA maneuver has been calculated and performed three times before the observer loses contacted with the observer. The various maneuvers allows the observer to maintain a more consistent track of the target.

This section also includes the error plots from experiment 6 as representative of the results from this set of speed ratio experiments. Figures 5.10, 5.11 and 5.12 contain these plots. This set of experiments does not have the same set of large errors that is typical of most of the geometry experiments. As stated previously, this is due to the specific geometry of these experiments. There is a jump in the speed and course errors of trial 1, which is consistent through all of the speed ratios. Therefore, the cause of this jump is within the random variables in either the initial estimate or in the noise statistics. In addition to these plots, Table 5.6 contains the errors within the information that the observer reports when it loses contact with the target. The mean percentage range errors are 20.4 percent, 13.7 percent and 50.5 percent for experiments 2, 6 and 7 respectively.

As can be seen in Table 5.6, experiment 6 has the best performance over all of its trials. In some ways this is expected since the observer has the ability to keep up with

Experiment	Trial 1	Trial 2	Trial 3	Trial 4	Trial 5	Average
2	926 s	908 s	917 s	871 s	909 s	906 s
6	2274 s	2344 s	2299 s	1423 s	3600 s [1]	2380 s
7	2025 s [2]	1517 s	1541 s	1873 s [3]	1521 s	1695 s

[1]The target never moves out of range in this trial

[2]The observer reaquires the target from 3150s - 3326s

[3]The observer reaquires the target from 2034s - 2152s and from 2565s - 2739s

Table 5.5: Nominal Speed Detection Loss. The time for each trial at which the target leaves the observer's sensor range, and the average for each experiment.

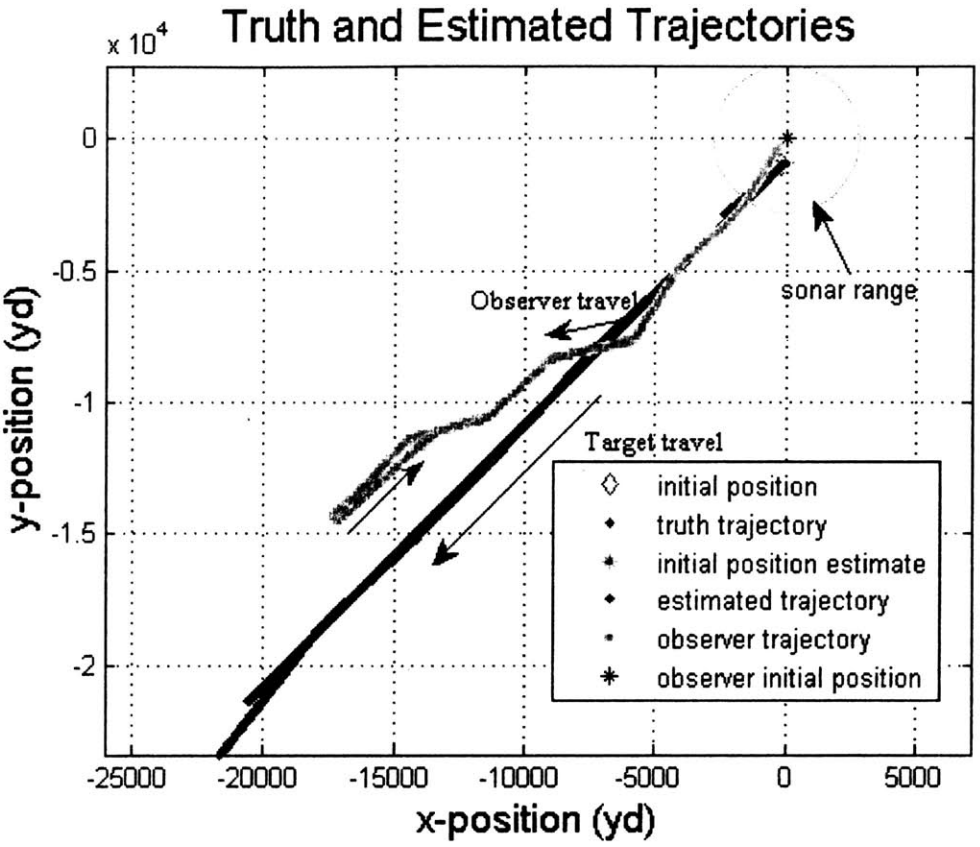

Figure 5.9: Experiment 6: Observer and Target Trajectories

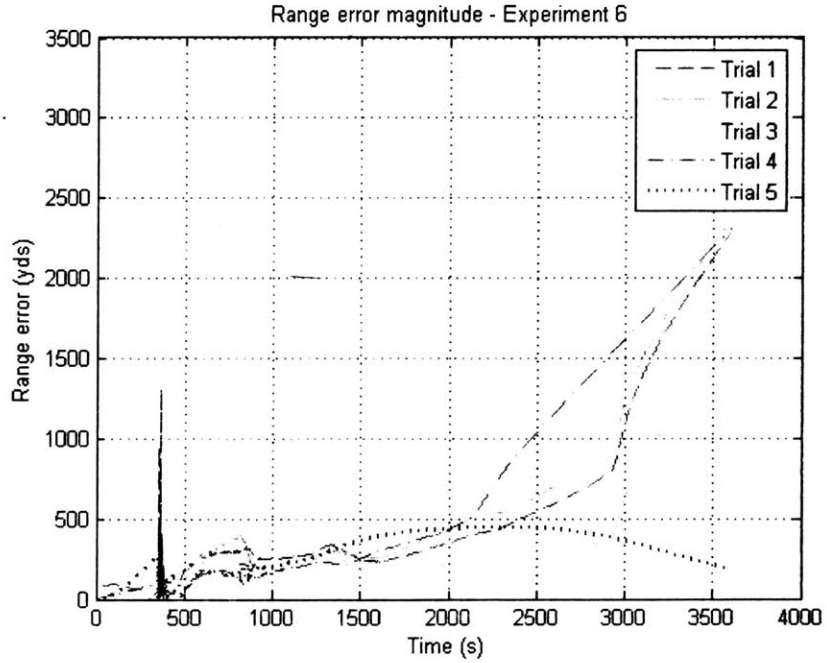

Figure 5.10: Range Error Plot

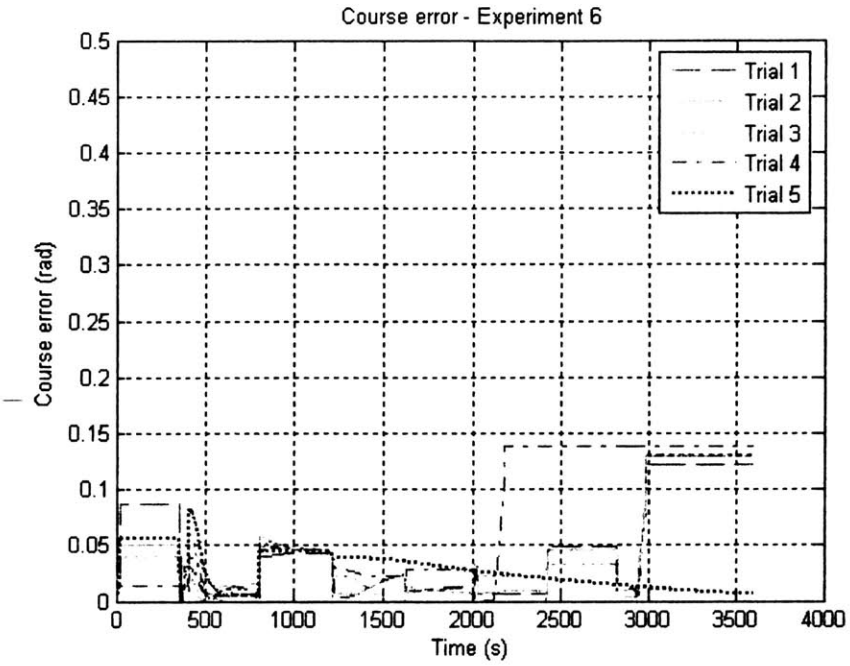

Figure 5.11: Course Error Plot

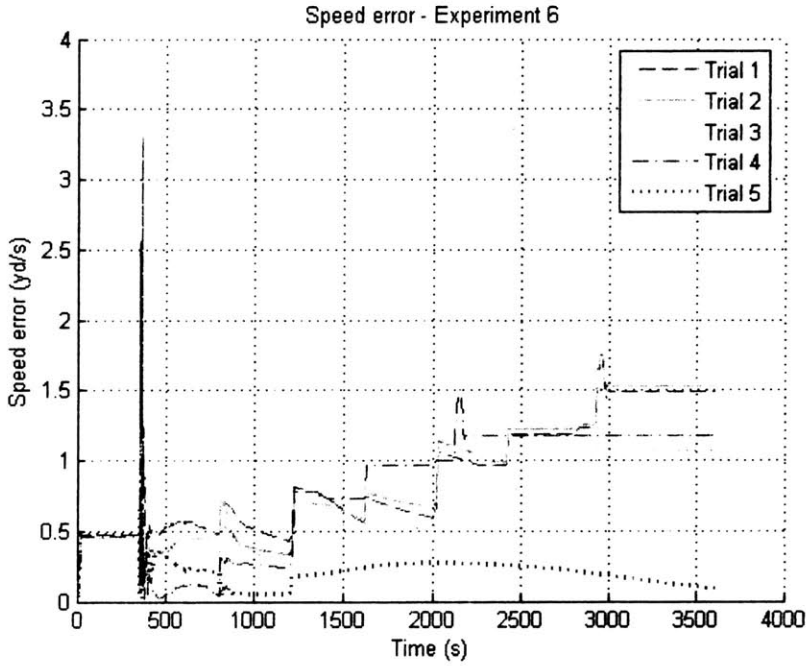

Figure 5.12: Speed Error Plot

	Range Errors (yds)					
Experiment	Trial 1	Trial 2	Trial 3	Trial 4	Trial 5	Ave
2	603	536	623	404	674	568
6	430	543	177	213	181	309
7	5900	132	848	125	25	1406
	Course Errors (rad)					
Experiment	Trial 1	Trial 2	Trial 3	Trial 4	Trial 5	Ave
2	0.0260	0.0336	0.0318	0.0381	0.0348	0.0329
6	0.00642	0.00968	0.0232	0.0224	0.00619	0.0136
7	0.0557	0.0597	0.0224	0.00137	0.0450	0.0368
	Speed Errors (yd/s)					
Experiment	Trial 1	Trial 2	Trial 3	Trial 4	Trial 5	Ave
2	0.885	0.797	0.777	0.617	0.399	0.695
6	0.960	0.989	0.602	0.730	0.0869	0.674
7	4.185	0.529	2.931	0.256	0.606	1.701

Table 5.6: Errors in Reported Information: Nominal Speed

the target when they are moving at the same speed. The observer also performed better when it was moving slower than the target rather than when it was moving faster (experiment 2 vs. experiment 7). However, the errors from experiment 7 when the observer has lost the target after reaquiring it are not included in Table 5.6. Other than an improvement in the range error in trial 1, there is not much improvement in the errors once the observer loses the target once again.

Table 5.7 presents the y state errors and covariances for each of the three speed ratio experiments at the initial loss of contact. Unlike experiment 2, the errors of the other two experiments typically fall outside of the bounds of the covariance. The errors in experiment 6 are usually about an order of magnitude greater than the covariance while those in experiment 7 are typically two orders of magnitude greater. Therefore, from these results, experiment 6 performs better than experiment 7.

	Bearing Rate Errors (rad/s)($\times 10^{-5}$) **Bearing Rate Covariance (σ)($\times 10^{-5}$)**					
Experiment	Trial 1	Trial 2	Trial 3	Trial 4	Trial 5	Mean
2	-1.57	-1.10	-1.74	0.208	-2.12	1.35
	14.3	17.5	16.0	28.9	18.1	19.0
6	18.3	19.0	13.2	-15.7	6.56	14.6
	0.326	0.359	0.418	0.500	0.706	0.462
7	-182.5	-13.6	-8.09	-0.661	-15.0	44.0
	0.142	0.429	0.152	1.32	0.382	0.485
	Bearing Errors (rad) **Bearing Covariance (σ)**					
Experiment	Trial 1	Trial 2	Trial 3	Trial 4	Trial 5	Mean
2	-0.0021	-0.0012	-0.0021	-0.0017	-0.0038	0.0022
	0.0149	0.0158	0.0153	0.0172	0.0158	0.0158
6	0.0878	0.0962	0.0775	-0.0339	0.0299	0.0651
	0.0037	0.0039	0.0040	0.0050	0.0048	0.0043
7	-0.6907	-0.0485	-0.8089	-0.0283	-0.0614	0.3276
	0.0016	0.0053	0.0047	0.0062	0.0051	0.0046
	Normalized Range Rate Errors (1/s)($\times 10^{-5}$) **Normalized Range Rate Covariance (σ)($\times 10^{-5}$)**					
Experiment	Trial 1	Trial 2	Trial 3	Trial 4	Trial 5	Mean
2	12.2	10.9	8.14	8.57	-4.48	8.85
	4.18	4.14	4.93	5.32	8.15	5.34
6	-0.465	-2.81	-3.36	7.68	7.33	4.33
	0.484	0.494	0.553	2.27	1.10	0.980
7	33.7	-2.38	79.1	-7.49	-.868	24.7
	0.130	0.733	0.350	0.518	0.695	0.485
	Reciprocal of Range Errors (1/yd)($\times 10^{-5}$) **Reciprocal of Range Covariance (σ)($\times 10^{-5}$)**					
Experiment	Trial 1	Trial 2	Trial 3	Trial 4	Trial 5	Mean
2	-6.38	-5.79	-6.56	-4.55	-6.99	6.05
	9.12	11.0	10.1	17.9	11.3	11.9
6	-4.80	-5.86	-2.14	-2.55	-12.2	5.51
	0.212	0.203	0.254	1.00	2.19	0.772
7	-68.0	-1.62	15.7	1.68	-0.314	17.5
	0.0389	0.297	0.115	1.05	0.269	0.354

Table 5.7: Y State Errors and Covariances for Nominal Case Speed Ratios

5.3 Worst Case Speed Experiments

These experiments have a similar set-up to those in the last section. The only difference is the environment in which the experiment is performed. Instead of the observer being in the nominal, every day environment, it is now in the worst environment. The main effect that the environment has on the observer is the reduction in the range of the sensor. Table 5.8 contains the time of detection loss for each of the three experiments. Due to the reduction of the sensor range, the observer never detects the target in experiments 8 and 9. The increase in speed is necessary for the observer to come close enough for the target to be within range of its sensors.

Since the observer does not detect the target in either experiment 8 or 9, the filter just propagates the initial estimate passed to the observer by the sensing network. The speed and the course errors are constant after the observer's initial maneuver to attempt to intercept the target. Due to these constant errors, the range error has a constant growth. Experiment 10 typically performs fairly well prior to losing contact with the target. After the loss of contact, if there is a significant error in the speed, this will manifest itself as a large range error. Table 5.9 presents the x state errors for these experiments. Since the target was never detected in the first two experiments, the range error was the initial estimate error and the speed and course errors are the constant errors that occured after the intercept maneuver. The errors for experiment 10 are those at the instant that the observer lost contact. In experiments 8 and 9, the mean percentage range error is 4.3 percent while experiment 10 mean range error is 14.1 percent of the true range value.

In addition to the x state errors, the y state errors and covariances are also tabulated. Since there are no maneuvers in either experiment 8 or 9, there are no sharp dips within the covariances. The covariance of the bearing between the target and observer continually grows since there are no bearing measurements. The errors and covariances for experiment 8 can be seen in Figures 5.13 and 5.14. The point at which the errors and covariances are measured for these two experiments is the instant before it settles to a constant speed and course error. The errors and covariances for experiment 10 are calculated at the point at which the observer loses contact with the target. These values are included in Table 5.10.

Since there are no maneuvers in either of the first two experiments of this set, the errors remain within the covariance bounds. The bearing errors are typically smaller in experiment 10 since it is receiving bearing measurements unlike the other two experiments. It is difficult to compare the errors between the different experiments

Experiment	Trial 1	Trial 2	Trial 3	Trial 4	Trial 5	Average
8	0 s	0 s	0 s	0 s	0 s	0 s
9	0 s	0 s	0 s	0 s	0 s	0 s
10	857 s	838 s	833 s	618 s	844 s	798 s

Table 5.8: Worst Case Speed Detection Loss. The time for each trial at which the target leaves the observer's sensor range, and the average for each experiment.

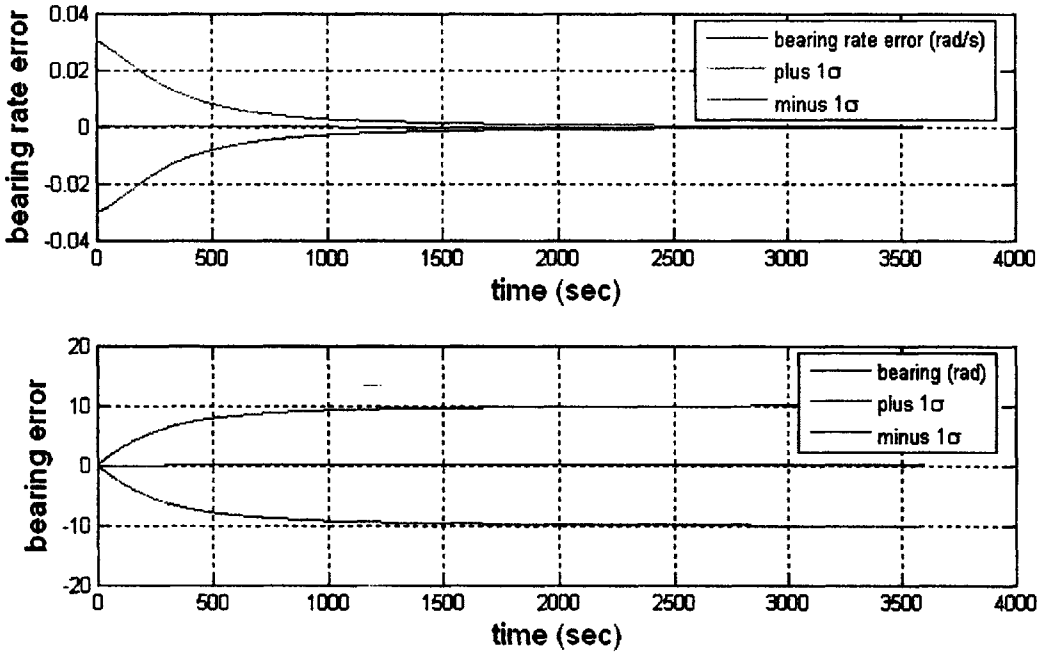

Figure 5.13: Bearing and Bearing Rate Errors and Covariance for Experiment 8

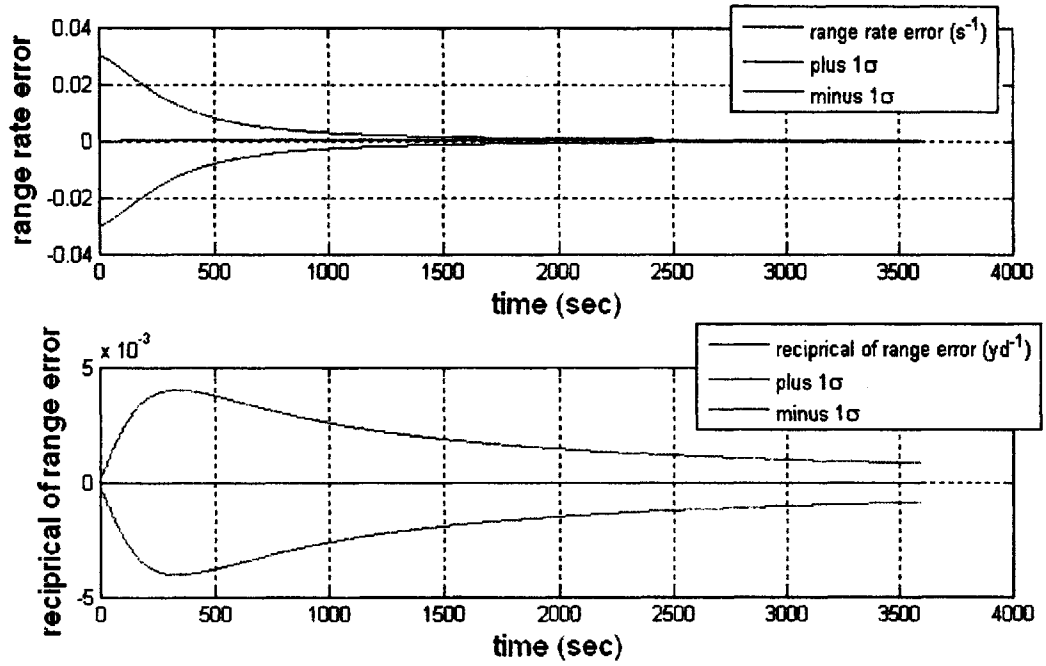

Figure 5.14: Normalized Range Rate and Reciprocal of Range Errors and Covariance for Experiment 8

	Range Errors (yds)					
Experiment	Trial 1	Trial 2	Trial 3	Trial 4	Trial 5	Ave
8	79	12	113	1	12	43
9	79	12	113	1	12	43
10	448	360	367	42	3967	1037
	Course Errors (rad)					
Experiment	Trial 1	Trial 2	Trial 3	Trial 4	Trial 5	Ave
8	0.0744	0.0365	0.0336	0.0269	0.0407	0.0424
9	0.0867	0.0508	0.0409	0.0135	0.0556	0.0495
10	0.305	0.0496	0.150	0.0376	0.718	0.252
	Speed Errors (yd/s)					
Experiment	Trial 1	Trial 2	Trial 3	Trial 4	Trial 5	Ave
8	0.359	0.321	0.265	0.333	0.344	0.324
9	0.479	0.450	0.369	0.460	0.475	0.447
10	10.45	0.703	3.970	0.143	1.392	3.332

Table 5.9: Errors in Reported Information: Worst Case Speed

since the MPEKF never really starts running in the first two experiments. The estimates are propagated, but there are no measurement updates. The results from experiment 10 can be compared with those of experiment 7, since they have the same set-up but differ in the geometry. This will be further explored in the next section.

	Bearing Rate Errors (rad/s)($\times 10^{-5}$) **Bearing Rate Covariance (σ)($\times 10^{-5}$)**					
Experiment	Trial 1	Trial 2	Trial 3	Trial 4	Trial 5	Mean
8	76.5	22.6	60.8	-12.6	4.75	35.5
	2951	2951	2923	2914	2910	2930
9	63.3	16.5	56.5	-16.0	40.3	38.5
	3117	3115	3101	3093	3104	3106
10	344.7	-67.5	-68.6	3.42	-58.3	108.5
	52.4	10.9	14.5	42.1	10.6	26.1
	Bearing Errors (rad) **Bearing Covariance (σ)**					
Experiment	Trial 1	Trial 2	Trial 3	Trial 4	Trial 5	Mean
8	-0.0937	-0.0902	-0.0343	-0.0730	0.1396	0.0862
	0.5695	0.5998	0.5671	0.6252	0.5987	0.5921
9	-0.0964	-0.0903	-0.0369	-0.0729	0.1443	0.0822
	0.5812	0.6121	0.5801	0.6395	0.6150	0.6056
10	0.0841	0.0550	0.0271	-0.0036	0.0538	0.0447
	0.0189	0.0132	0.0135	0.0191	0.0127	0.0155
	Normalized Range Rate Errors (1/s)($\times 10^{-5}$) **Normalized Range Rate Covariance (σ)($\times 10^{-5}$)**					
Experiment	Trial 1	Trial 2	Trial 3	Trial 4	Trial 5	Mean
8	-17.5	-8.18	10.3	2.27	51.6	18.0
	2953	2952	2924	2914	2909	2930
9	-22.5	3.70	-4.84	34.1	50.1	23.0
	3119	3118	3103	3094	3102	3107
10	-914.1	-131.8	-447.5	-34.5	-205.9	346.8
	49.3	4.98	10.1	89.4	6.27	32.0
	Reciprocal of Range Errors (1/yd)($\times 10^{-5}$) **Reciprocal of Range Covariance (σ)($\times 10^{-5}$)**					
Experiment	Trial 1	Trial 2	Trial 3	Trial 4	Trial 5	Mean
8	7.82	-0.857	11.2	-0.435	1.16	4.29
	65.2	63.3	66.6	65.5	64.1	64.9
9	7.93	-1.09	11.6	-0.618	1.60	4.57
	67.9	65.9	69.6	68.4	70.2	68.4
10	-51.7	-44.9	-45.4	8.19	-114.8	53.0
	10.4	6.98	7.08	44.3	6.62	15.1

Table 5.10: y State Errors and Covariances for Worst Case Speed Ratios

5.4 Nominal Case vs Worst Case

The final set of experiments consisted of an additional run of experiment 4 in the worst case environment. This allows for a comparison of the two different geometries. In addition, the results from experiments 7 and 10 will be compared. Table 5.11 presents the times at which the target leaves the observer's detection range. This demonstrates the degredation that is caused by the decreasing sensor range. This reduction in detection time is consistent with that seen between experiments 7 and 10 as well.

The actual and estimated trajectories for experiment 11 are presented in Figure 5.15. The main differences in the observer trajectories between the two experiments are due to the difference in the sonar range. As seen in Figure 5.15, the observer travels on the initial intercept course for a length of time before the target comes into range. In experiment 4, on the other hand, the target is within range of the observer almost at the beginning of the run. Experiment 11 does not have the initial errors that are present in experiment 4 (similar to those in Figures 5.2, 5.3 and 5.4 at the beginning of the chapter). This is due to the fact that there is a different bearing angle between the observer and the target when the BO-TMA is initialized and the filter begins updating the measurements. The observer is not taking measurements when the bearing crosses the 0 radian mark in experiment 10.

The range, course and speed errors for experiments 4 and 10 are presented in Table 5.12. From this table it can be seen that experiment 11 performs better in the absolute estimation of the range, however the mean percent range error for experiment 10 is 21.9 percent while it is only 14.8 percent for experiment 4. Experiment 4 also performs better in the course and speed estimation. Similar results are seen when experiments 7 and 10 are compared. The course and speed estimates are better in the nominal environment while the range estimate is better in the worse environment.

The figures of the covariance and y state errors for experiment 4 are presented earlier in this chapter in Figures 5.5, 5.6, 5.7 and 5.8. The covariance is not reduced as quickly in experiment 11. The effects of the maneuvers can be seen fairly well in the initial covariance plot prior to the zoom in. This can also be observed within the results in Table 5.13. The mean covariance for each variable in experiment 11 is much larger than those for experiment 4. The errors are also larger in experiment 11 than experiment 4 at the time of detection loss. This also holds true when comparing the y state errors and covariances between experiments 7 and 10. The only point at which it breaks down is within the bearing errors. The mean bearing error is smaller for experiment 10 than it is for experiment 7.

Experiment	Trial 1	Trial 2	Trial 3	Trial 4	Trial 5	Average
4	1785 s	1831 s	1814 s	1915 s	1832 s	1835 s
11	662 s	577 s	612 s	544 s	581 s	595 s

Table 5.11: Nominal vs. Worst Case Detection Loss. The time for each trial at which the target leaves the observer's sensor range, and the average for each experiment.

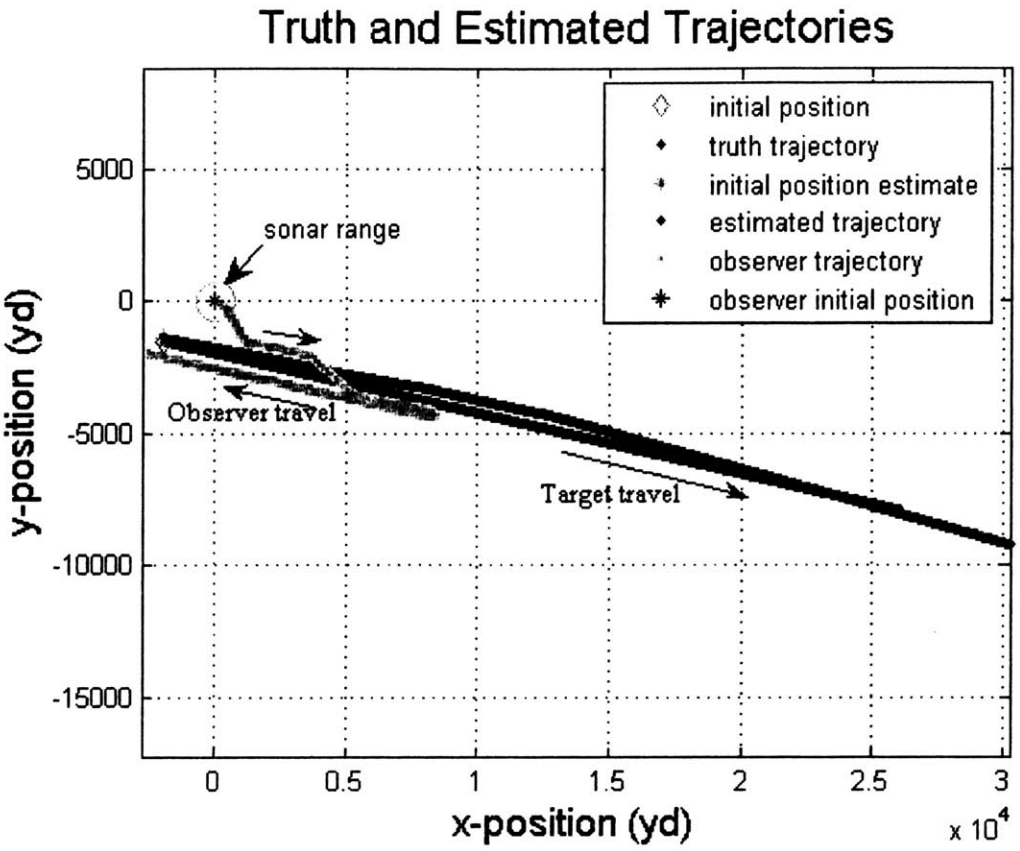

Figure 5.15: Experiment 11: Observer and Target Trajectories

	Range Errors (yds)					
Experiment	Trial 1	Trial 2	Trial 3	Trial 4	Trial 5	Ave
4	102	351	514	697	401	413
11	318	86	54	258	89	161
	Course Errors (rad)					
Experiment	Trial 1	Trial 2	Trial 3	Trial 4	Trial 5	Ave
4	0.0517	0.0234	0.00159	0.0126	0.0166	0.0212
11	0.0236	0.0180	0.0194	0.0748	0.0134	0.0298
	Speed Errors (yd/s)					
Experiment	Trial 1	Trial 2	Trial 3	Trial 4	Trial 5	Ave
4	0.443	0.622	0.758	0.538	0.645	0.601
11	0.748	0.909	0.807	0.704	0.915	0.817

Table 5.12: Errors in Reported Information: Nominal vs. Worst Case

	Bearing Rate Errors (rad/s)($\times 10^{-5}$) **Bearing Rate Covariance (σ)($\times 10^{-5}$)**					
Experiment	Trial 1	Trial 2	Trial 3	Trial 4	Trial 5	Mean
4	14.9	6.88	2.22	2.87	5.08	6.39
	1.66	1.50	1.33	0.549	1.44	1.30
11	102.5	70.2	62.9	-77.5	-53.1	73.2
	7181	12300	13600	38500	25600	19400
	Bearing Errors (rad) **Bearing Covariance (σ)**					
Experiment	Trial 1	Trial 2	Trial 3	Trial 4	Trial 5	Mean
4	0.0344	0.0194	0.0097	0.0110	0.0171	0.0183
	0.0045	0.0047	0.0045	0.0051	0.0045	0.0047
11	-0.4412	-0.7246	-0.6703	-0.8581	-0.5086	0.6406
	47.11	54.22	58.60	88.15	73.44	64.30
	Normalized Range Rate Errors (1/s)($\times 10^{-5}$) **Normalized Range Rate Covariance (σ)($\times 10^{-5}$)**					
Experiment	Trial 1	Trial 2	Trial 3	Trial 4	Trial 5	Mean
4	9.61	10.9	11.6	2.45	10.6	9.03
	0.436	0.256	0.299	0.293	0.263	0.309
11	89.5	192.9	185.5	346.8	222.5	207.4
	7202	12400	13600	38600	25600	19500
	Reciprocal of Range Errors (1/yd)($\times 10^{-5}$) **Reciprocal of Range Covariance (σ)($\times 10^{-5}$)**					
Experiment	Trial 1	Trial 2	Trial 3	Trial 4	Trial 5	Mean
4	-1.27	-4.01	-5.58	-7.18	-4.51	4.51
	0.882	0.827	0.768	3.16	0.817	1.29
11	-41.1	-14.2	-9.35	73.3	18.8	31.4
	4493	6634	7450	18500	14400	9706

Table 5.13: y State Errors and Covariances for Nominal vs Worst Case

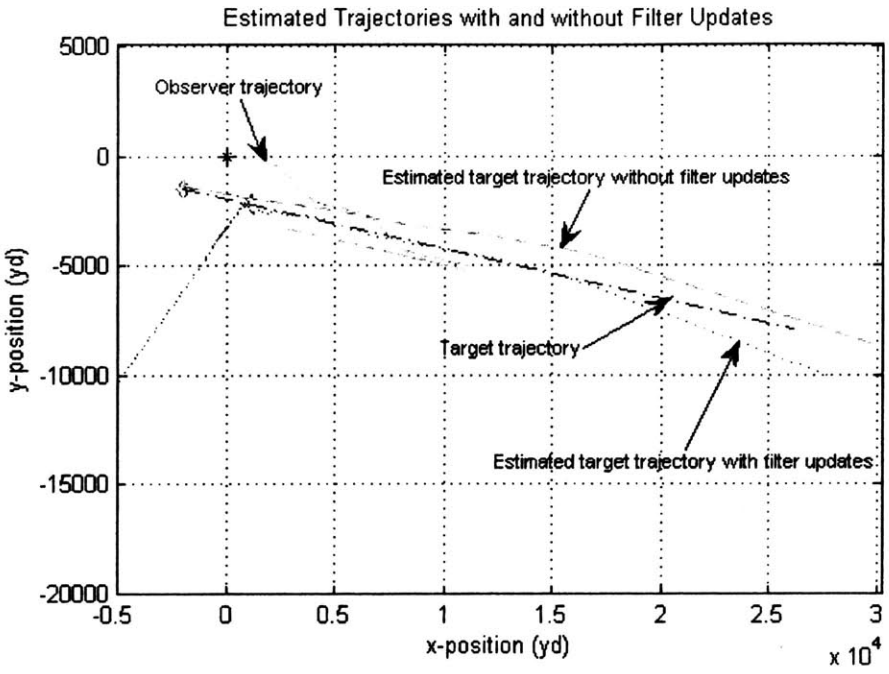

Figure 5.16: Experiment 4: Observer and Target Trajectories

Figure 5.16 demonstrates the effects of the filter updates on the estimation. This figure plots the true target trajectory, the estimated trajectory with the filter turned on, the estimated trajectory with the filter turned off and the observer trajectory for experiment 4. This trial calculates both the updated and non updated estimates of the target state. The observer trajectory is based on the updated estimates, while the non updated estimates are affected by the observer's maneuvers. This figure demonstrates that the MPEKF improves the estimate with the updates based on the measurements. The point at which the estimate trajectory with filter updates diverges from the truth trajectory occurs when the observer has turned around after it has lost contact with the target.

To briefly sum up, certain geometries performed better than others. In addition, the observer having an identical speed as the target improved the performance of an otherwise lacking geometry. Working in the worst case environment decreased the length of time, if any, that the observer received measurements from the target. Further conclusions from these results will be drawn in the next chapter.

Chapter 6

Conclusion

Unmanned underwater vehicles (UUVs) are becoming more prominent in various areas of the civilian, military and research sectors. They have an ability to expand access to one of earth's most unknown environments, the ocean. UUVs can augment the work that is currently done in the underwater environment.

Specifically, UUVs have a variety of missions they can accomplish in littoral areas that are not easily accomplished by larger vessels. This thesis examines the development of a guidance algorithm for use in these areas. One particular mission to be accomplished in the littoral area of the ocean is the tracking of vessels leaving a port or coming through a check point. In order for a UUV to track without being detected, it must perform passive bearings-only tracking.

This thesis presents a guidance algorithm for UUVs to perform bearings-only tracking. Chapter 3 includes the development of this guidance algorithm. As a part of this development, specific maneuver experiments are conducted. These experiments confirm the ability to perform bearings-only tracking. The experiments allow for an observation of the effectiveness of a variety of maneuvers that will provide the backbone for the guidance logic.

Chapter 5 presents the results from a variety of situations using this guidance logic. Each run in itself demonstrates that the guidance logic performs bearings-only tracking. These situations vary the initial geometry of the observer and target, the speed ratios between the observer and target and the environment in which they are both operating. Each of these sets of experiments explores a different aspect of the bearings-only tracking problem.

The first set of experiments explored the effects of the initial geometry of the target and observer. These geometries correspond to various points where the observer is cued to track the target. The least effective geometry is that in which the observer does not begin to track the target until the target is already ahead of the observer and moving away as can be seen in the results from experiment 2. In this case ahead means that the target is moving away from the observer along the bearing between the observer and target. The observer is always trying to catch up with the target and quickly loses contact with it in this geometry. The geometries of experiments 1, 3 and 4 are similiar in their respective positions but vary in the initial relative course of the observer. Experiments 1 and 4 perform more consistantly than experiment 3. This

might be due to the fact that experiment 3's initial intercept course is perpindicular to the target's course, unlike the other two experiments. Experiment 5 has a vastly different geometry in that observer begins out ahead of the target and its initial course is in the general direction of the target. This allows the observer to maintain contact with the target for a longer period of time since it begins tracking the target before the target has passed it.

From the results, some general guidelines can be determined for the positioning of the observer. The observer should be outside of the harbor or chokepoint that it is monitoring. For better results, the UUV should be cued before the target will have passed its position. When the UUV is either off to the side of the target or heading on a reciprocal course, it performs better than when the target has already passed as it begins to track the target.

The second set of experiments explores the effect of the speed ratio on the effectiveness of the observer's tracking. The geometry that is used is the least effective geometry, in order to determing if changing the speed ration would improve its performance. In this situation, the observer was most effective when it moved at the same speed as the target. The performance at the same speed is comparable to the UUV's performance in the other geometries at a slower speed. Somewhat counterintuitively, the observer performed better when it was moving slower than the target rather than faster. This is due to the fact that the observer quickly passes the target and loses contact with the target when it is moving faster. When the observer is slower than the target, it follows the target until the target moves out of range. However, it is unlikely that the UUV would be able to travel faster than the target vessel. In most situations, the UUV would travel slower or possibly the same speed as the vessel in the restricted waters. The UUV would not have the same speed capabilities as the target. In general UUVs are slower than the type of vessels they would be tracking. In restricted waters, the UUV might travel at the same speed if the target has more speed restrictions than the UUV. Once the vehicles entered open water, the target vessel would probably speed up and the UUV would not be able to maintain a track for the entire time.

In the third set of experiments, the speed ratio is varied again, but this time in the worst case acoustic environment. In this undesirable environment, the UUV never even detects the target in the first two situations. The UUV needs to be at the top speed in order to come within range of the target. This also demonstrates the ineffectiveness of the second geometry in an extremely noisy environment.

The final set of experiments compares the nominal environment to the worst case environment. The results indicate that the fourth geometry is somewhat effective in the noisy acoustic environment. The UUV is able to track the target for short period of time before the target moves out of range. This indicates that it is possible to use the UUV in less than desirable weather and areas.

The results from each of the experiments indicates that autonomous bearings-only tracking is feasible. However, further work needs to be done before this algorithm can be implimented on a real UUV. This further work will be explored in the next section.

6.1 Further Work

This section presents an overview of further work that needs to be complete prior to having a working UUV that performs autonomous bearings-only tracking. The guidance algorithm that has been presented in this thesis only takes into account the current states of both the observer and the target. The next step would be to enable the observer to avoid obstacles while performing the BO-TMA.

Obstacle avoidance for UUVs is currently being explored by various organizations. There is room for continuing work in combining low level obstacle avoidance with target tracking. The UUV will have to maneuver around objects while trying to maintain its track of the target. In order to maintain the track of the target, or at least to keep the target within range, the observer should try to prevent obstacles from obstructing its ability to sense the target. One possible method is to always move towards the target when avoiding an obstacle.

In addition to obstacle avoidance, the guidance algorithm can be improved to account for target maneuvers. There are two aspects to the target maneuvers. The first is that the filter is designed under the assumption that the target has a constant course and speed. The UUV would either have to start the BO-TMA over again after a maneuver, inject a process noise transient or have a more accurate model of the target. The other aspect of target maneuvers is the determination of counter detection. This aspect has been explored in Mierisch's work [19].

Further extensions of this work include combining with the navigation of ownship, contact classification, online optimization of track versus trail and explicitly accounting for power and fuel. This thesis assumes that the observer knows its own position perfectly. Further extensions of the work would be to account for errors in the observer's self knowledge. In addition, this thesis solely focuses on the specific guidance for the BO-TMA maneuvers. This guidance needs to be folded into the main navigation system of the ownship that controls the entire mission of the observer, from launch to recovery.

Another extension is contact classification. This would allow for the UUV to be more discriminate in the contacts that it tracks. If the sensor network cues it to a target, the observer can determine if the contact is one of interest or not. This would allow the UUV to have a longer station time in which the observer does not track every target that it has been alerted of.

This thesis presents a modest guidance algorithm. This could be further improved to allow for online optimization between tracking the target and trailing the target. Currently, the angles of the maneuvers are set in the algorithm. The online optimization would allow for more variety in the maneuvers and improve their performance. In addition, the optimization could be used to improve the BO-TMA performance when encountering obstacles.

The final area in the control of the UUV that should be explored is the accounting of the power and fuel available. The levels of power and fuel are important to the navigation and control of the vehicle. These levels dictate whether or not the UUV is able to wait for another contact. Work needs to be done in incorporating these inputs into the higher level control system of the UUV.

In order to for the UUV to perform this mission for the required length of time, there needs to be more research into power sources and supplies. Current sources do not last long enough for the main goals of this mission. Bearings-only tracking requires the UUV to have a long lasting power source in order to track different targets without having to return recharge after each track.

Another area of ongoing research is in the underwater sensors themselves. The range of the sensors greatly affects the effectiveness of the UUV. Underwater is a complicated and noisy environment. The noise levels vary and it is difficult to predict the operation of the sensors from day to day. There has been much research in other types of sensors other than acoustic sensors. These could help to increase the range in which a UUV could detect another vessel.

Other areas of research to accomplish this mission include underwater communications and cooperation. The UUV needs to be able to communicate with the sensor field that cues it as well as be able to send its aquired information to its home platform. Underwater communications and cooperation is a current and vibrant area of research. More than likely a sensor net would have multiple UUVs waiting to cued to track an outgoing vessel. If this is the case, those UUVs must be able to cooperate with each other and communicate with each other. This area is an important aspect of implementing bearings-only tracking as part of a force multiplier in a communication network in littoral areas.

Bibliography

[1] Vincent J. Aidala and Sherry E. Hammel. Utilization of Modified Polar Coordinates for Bearings-Only Tracking. *IEEE Transactions on Automatic Control*, AC-28(3):283–294, Mar 1983.

[2] Klaus Becker. Simple Linear Theory Approach to TMA Observability. *IEEE Transactions on Aerospace and Electronic Systems*, 29(2):575–578, Apr 1993.

[3] Klaus Becker. A General Approach to TMA Observability from Angle and Frequency Measurements. *IEEE Transactions on Aerospace and Electronic Systems*, 32(1):487–494, Jan 1996.

[4] Klaus Becker. Target Motion Analysis (TMA). In Stergios Stergiopoulos, editor, *Advanced Signal Processing Handbook: Theory and Implementation for Radar, Sonar, and Medical Imaging Real-Time Systems*, chapter 9, pages 9.1–9.21. CRC Press, Boca Raton, Florida, 2001.

[5] Zeev Berman. A Reliable Maximum Likelihood Algorithm for Bearing-Only Target Motion Analysis. In *Proceedings of the 36th Conference on Decision and Control*, pages 5012–5017, Dec 1997.

[6] J. P. Le Cadre and Olivier Trémois. Optimization of the Observer Motion using Dynamic Programming. *IEEE Transactions on Acoustics, Speech and Signal Processing*, pages 3567–3570, May 1995.

[7] Jean-Pierre Le Cadre and Olivier Trémois. Bearings-Only Tracking for Maneuvering Sources. *IEEE Transactions on Aerospace and Electronic Systems*, 34(1):179–193, Jan 1998.

[8] Alfonso Farina. Target Tracking with Bearings-Only Measurements. *Signal Processing*, 78:61–78, Mar 1999.

[9] John A. Fawcett. Effect of Course Maneuvers on Bearings-only Range Estimation. *IEEE Transactions on Acoustics, Speech, and Signal Processing*, 36(8):1193–1199, Aug 1988.

[10] Eli Fogel and Motti Gavish. Nth-Order Dynamics Target Observability From Angle Measurements. *IEEE Transactions on Aerospace and Electronic Systems*, 24(3):305–308, May 1988.

[11] T. H. Frank, J. W. Kesner, and H. M. Gruen. Conformal array beam patterns and directivity indices. *The Journal of the Acoustical Society of America*, 63(3):841–847, 1978.

[12] Arthur Gelb, editor. *Applied Optimal Estimation.* MIT Press, Cambridge, MA, 1974.

[13] Sherry E. Hammel. *Optimal Observer Motion for Bearings-Only Localization and Tracking.* Applied mathematical sciences, University of Rhode Island, 1988.

[14] Sherry E. Hammel, Vincent J. Aidala, Kai F. Gong, and Allen G. Lindgren. Recursive versus Batch Processing Algorithms for Bearings-Only Tracking. In *OCEANS '83 Conference Proceedings*, volume 15, pages 50–61, Aug 1983.

[15] Claude Jauffret and Denis Pillon. Observability in Passive Target Motion Analysis. *IEEE Transactions on Aerospace and Electronic Systems*, 32(4):1290–1300, Oct 1996.

[16] Thomas Kailath. *Linear Systems.* Prentice Hall, NJ, 1980.

[17] T. R. Kronhamn. Bearings-Only Target Motion Analysis Based on a Multihypothesis Kalman Filter and Adaptive Ownship Motion Control. *IEE Proceedings - Radar, Sonar Navigation*, 145(4):247–252, Aug 1998.

[18] Xavier Lurton. *An Introduction to Underwater Acoustics: Principles and Applications.* Praxis Publishing Ltd, Chichester, UK, 2002.

[19] Andrew P. Mierisch. Situational Awareness for a Navy Unmanned Undersea Vehicle. Master's thesis, Department of Electrical Engineering and Computer Science, Massachusetts Institute of Technology, 2003.

[20] Martin J. Moorman and Thomas E. Bullock. A New Estimator for Passive Tracking of Maneuvering Targets. In *First IEEE Conference on Control Applications*, pages 1122–1127, Sep 1992.

[21] Steven C. Nardone and Marcus L. Graham. A Closed-Form Solution to Bearings-Only Target Motion Analysis. *IEEE Journal of Oceanic Engineering*, 22(1):168–178, Jan 1997.

[22] Steven C. Nardone, Allen G. Lindgren, and Kai F. Gong. Fundamental Properties and Performance of Conventional Bearings-Only Target Motion Analysis. *IEEE Transactions of Automatic Control*, AC-29(9):775–787, Sep 1984.

[23] Office of Naval Research. Science and Technology Focus: Oceanography: Ocean Regions, April 2004. http://www.onr.navy.mil/Focus/ocean/regions/default.htm.

[24] J. M. Passerieux and D. Van Cappel. Optimal Observer Maneuver for Bearings-Only Tracking. *IEEE Transactions on Aerospace and Electronic Systems*, 34(3):777–788, Jul 1998.

[25] Dinh Tuan Pham. Some Quick and Efficient Methods for Bearing-Only Target Motion Analysis. *IEEE Transactions on Signal Processing*, 41(9):2737–2751, Sep 1993.

[26] Olivier Trémois and J. P. Le Cadre. Maneuvering Target Motion Analysis Using Hidden Markov Model. *IEEE Transactions on Acoustics, Speech and Signal Processing*, pages 317–320, Apr 1994.

[27] Edward J. Tucholski et al. *US Naval Academy, Underwater Acoustics and Sonar (SP411), Course Notes.* USNA Physics Department, 2006. http://usna.edu/Users/physics/ejtuchol/.

[28] Robert J. Urick. *Principles of Underwater Sound.* McGraw-Hill Book Company, New York, third edition, 1983.

[29] US Navy. *The Navy Unmanned Undersea Vehicle (UUV) Master Plan*, November 2004. http://www.chinfo.navy.mil/navpalib/technology/uuvmp.pdf.

[30] Daniel H. Wagner, W. Charles Mylander, and Thomas J. Sanders, editors. *Naval Operations Analysis.* Naval Institute Press, Annapolis, MD, third edition, 1999.